



# Thermodynamic and economic analysis of a novel multi-generation system integrating solid oxide electrolysis cell and compressed air energy storage with SOFC-GT

Bo Li<sup>a</sup>, Heng Chen<sup>a,\*</sup>, Jinhang Li<sup>a</sup>, Wenchao Li<sup>b,1</sup>, Peiyuan Pan<sup>a</sup>, Lining Wu<sup>a</sup>, Gang Xu<sup>a</sup>

<sup>a</sup> North China Electric Power University, Beijing 102206, China

<sup>b</sup> The Seventh Medical Center of Chinese People's Liberation Army General Hospital, Beijing 100853, China

## ARTICLE INFO

### Keywords:

Solid oxide fuel cell  
Hybrid power system  
Combined Heat, Power, and Hydrogen Production  
Peak shaving optimization  
Techno-economic model

## ABSTRACT

Traditional gas-fired power plants are characterized by low efficiency and challenges in peak regulation. Even with the incorporation of compressed air energy storage, they still exhibit deficiencies in flexibility during peak load regulation. In this paper, we propose a novel hybrid power system based on gas-fired power plants, capable of producing electricity, heat, and hydrogen, while achieving flexible peak load regulation. The system is comprehensively evaluated using energy analysis, exergy analysis, and economic analysis. Results show that the total energy efficiency and exergy efficiency of this hybrid power system perform well, surpassing existing research on fuel cell-gas turbine systems. Among the subsystems, the fuel cell contributes the most to the total energy output of the hybrid system but also incurs the highest exergy losses, while the relative exergy losses of the water electrolysis and compressed air energy storage systems are relatively small. The configuration of dual energy storage systems enhances the flexibility in peak load regulation. Additionally, the proposed hybrid system exhibits low carbon emissions of 0.08 to 0.12 t/GJ. Considering factors such as discount rate, the initial investment cost can be recovered in 5.81 years, and the calculated net present value is 492,275.82 k\$. Thus, the proposed scheme also possesses certain advantages in terms of economic feasibility.

## 1. Introduction

Energy is one of the critical factors in strengthening and building the national economy. With the increasing living standards and rapid economic development, humans' demand for energy supply is also increasing. Fossil fuels impose an increasingly heavy burden on the environment. Improving energy efficiency, reducing carbon emissions, and exploring the potential for new energy generation are important ways to solve the energy crisis [1]. However, there is significant uncertainty in the grid-connected new energy power generation, which poses a more significant challenge to the peak regulation capability of the power grid. At present, unit peak regulation still relies on deviations from the design operating conditions of thermal power units [2]. Therefore, current efforts are aimed at researching technologies that can achieve peak shaving processes without relying on polluting operations or deviating from the design conditions while also improving energy utilization efficiency and reducing carbon emissions from thermal

power plants. It seeks to explore lower-carbon, cleaner, and more efficient power generation technologies such as fuel cells or design multi-system integration to achieve cascaded energy utilization, which is an effective approach to improve energy utilization efficiency [3].

In comparison to traditional coal-fired power plants, gas-fired power plants possess higher thermal efficiency (38% – 42%) and operational flexibility, while natural gas combined cycle power plants exhibit thermal efficiency as high as 40% – 60%, and are more easily integrated with other power generation devices [4]. Among the various options available, solid oxide fuel cell (SOFC) is a particularly practical choice. SOFC can directly convert the chemical energy of various fuel gases, such as natural gas or biomass gas, into electricity. The combustion process in the proposed system demonstrates minimal pollutant emissions, thus enhancing its environmental friendliness [5]. Moreover, the operating temperature exceeding 800 °C ensures the supply of high-grade thermal energy (for heating or hot water production) to external users [6]. Dual-power systems offer a compact solution that enables higher power output within a reduced footprint, achieving power

\* Corresponding author.

E-mail address: [heng@ncepu.edu.cn](mailto:heng@ncepu.edu.cn) (H. Chen).

<sup>1</sup> These authors contributed to the work equally and should be regarded as co-first authors.

Nomenclature			
<i>Symbols</i>		el	Electrical
$A$	Active area	in	Inlet
$C$	Cash flow	net	Net electric power
$F$	Faraday constant	ph	Physical
$H_{H_2}$	High heat value of the hydrogen	th	Thermal
$i_c$	Current density	cons	Consumption
$k$	Project lifetime	dis	Discount
$m$	Flow rate	gas	Syngas
$n$	Molar flow rate	ms	Material stream
$P$	Pressure	out	Outlet
$R$	Universal gas constant	ref	Reference
$T$	Temperature	tot	Total
$V$	Voltage	<i>Abbreviations</i>	
$y$	Years	AB	Air blower
ASR	Area specific resistance	CAES	Compressed air energy storage
EX	Exergy	COMP	Compressor
$G$	Gibbs free energy	DC	Direct current
$I$	Current	DHW	Domestic hot water
$i_{dis}$	Discount rate	GE	Generator
LHV	Low heating value	HC	Hydrogen compressor
$N$	Number of individual cells	NPV	Net present value
$Ne$	Number of electrons	SOFC	Solid oxide fuel cell
$Q$	Quantity of heat	WP	Water pump
$R_g$	Gas constant	AC	Alternating current
$U_f$	Utilization factor	CC	Combustion chamber
$W$	Power	CON	Condenser
$\eta$	Efficiency	DPP	Dynamic payback period
<i>Superscripts and subscripts</i>		FC	Fuel compressor
ch	Chemical	GT	Gas turbine
des	Destruction	HE	Heat exchanger
		SOEC	Solid oxide electrolysis cell
		WHR	Waste heat recovery

generation efficiencies of up to 70% [7]. This efficiency surpasses that of single gas turbines or solid oxide fuel cells alone, making dual-power systems an attractive option [8]. So far, many scholars have studied the performance of fuel cell and gas turbine integrated systems, as well as the integration technology of SOFC-GT with other power supply systems, and have demonstrated that the SOFC-GT hybrid power system is a clean, efficient, and highly flexible technology with promising development prospects.

The authors Huang et al. [9] investigated the fuel sensitivity of a hybrid power system comprising a solid oxide fuel cell and gas turbine, and conducted an optimization analysis. They found that when methane is employed as fuel, the optimal electric efficiency is 56.1%. Chitgar et al. [10] proposed an integrated system that combined solid oxide fuel cell-gas turbine with multi-effect desalination, organic flash cycle, and polymer electrolyte membrane electrolytic cell to generate electricity, fresh water, and hydrogen simultaneously. The system is analyzed using Exergy economic analysis to evaluate its energy efficiency and cost-effectiveness performance. Pirkandi et al. [11] modelled and analyzed the thermodynamic performance of a hybrid system consisting of a steam turbine, gas turbine, and solid oxide fuel cell. Nine different cycle configurations are investigated to explore the optimal cycle based on thermodynamic performance. The study confirmed the significant increase in the electricity generation efficiency of such a system compared to a single system, thus validating the effectiveness of this model. In addition, numerous studies have proposed integrating solid oxide fuel cell-gas turbine (SOFC-GT) systems with other power generation technologies such as organic Rankine cycle, carbon capture and storage, and combined cooling, heating, and power systems [12–15].

Despite the significant improvement in power generation efficiency

achieved by the SOFC-GT hybrid power system, it still relies on system start-stop and operational adjustments to achieve peak regulation, which may present certain limitations and deficiencies. In addressing this issue, researchers have explored the integration of energy storage technologies into the SOFC-GT system [16]. The basic principle of energy storage technology is to store excess electricity in other forms during low-load periods and release it during peak power demand [17]. Pumped hydro storage is the most widely used mechanical energy storage technology, but it requires particular terrain and has stringent environmental requirements for construction [18]. Compressed air energy storage (CAES) is considered one of the most promising mechanical energy storage technologies, in addition to pumped hydro storage. With its advantages of large storage capacity, long storage time, high safety, strong reliability, and high coupling flexibility, CAES has become a widely studied and invested energy storage solution, with the goal of being widely applied in practical production [19].

Han et al. [20] proposed a coordinated optimization method for dynamically adjusting the energy output of a compressed air energy storage system integrated with various other systems, using genetic algorithms for analysis. Roushenas et al. [19] proposed a novel integration of the solid oxide fuel cell with the compressed air energy storage system. They conducted a comprehensive assessment of the system's performance through energy and exergy analyses, which proved the above excellent performance of CAES while also highlighting certain associated challenges. Similar issues are commonly observed in other existing research literature.

For instance, CAES systems for energy storage and peak regulation still face certain limitations, such as large spatial requirements, insufficient peak regulation depth, and slow response times [21]. From this

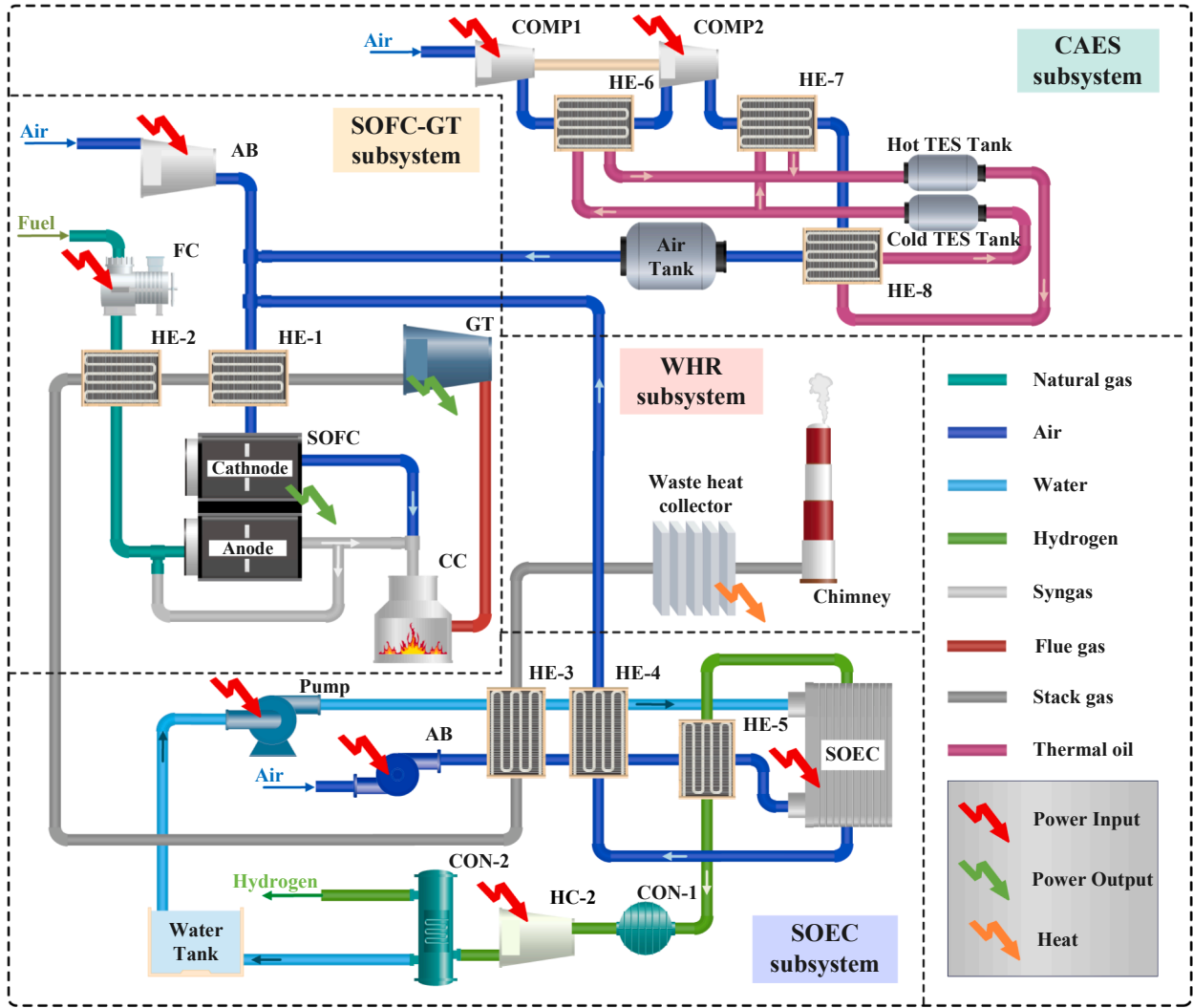


Fig. 1. Diagram of the hybrid system.

perspective, this study shifts focus towards hydrogen energy storage technology, employing it as an auxiliary peak regulation technique integrated with the SOFC system. By combining it with the existing CAES system, we aim to achieve enhanced peak regulation flexibility and depth in our hybrid power system.

Another reason for choosing hydrogen energy storage for peak shaving is that hydrogen, as one of the carriers of green energy, has a high calorific value and is clean. These characteristics make it have great potential for development in the future and become an efficient fuel [22]. In recent years, scholars have turned their attention to the development of hydrogen energy to alleviate the burden on the environment caused by the burning of fossil fuels. Many power plants have planned energy transformation and implemented collaborative hydrogen production programs [23–25].

With the development of hydrogen technology and its expanding application range, the market prospects for the hydrogen industry are becoming increasingly broad. At present, countries around the world have successively introduced a series of hydrogen-related policies and regulations, encouraging enterprises to invest in hydrogen research, production, and application to promote the development of the hydrogen industry [26–28]. According to the 2023 edition of 'BP World Energy Outlook' released by BP. Amoco, it is expected that by 2030, in the 'Rapid Transformation' and 'Net Zero' scenarios, the demand for low-carbon hydrogen will reach 30 to 50 million tons per year, of which green hydrogen will account for about 60% [29].

The technologies widely used in the hydrogen production industry chain include fossil fuel-based hydrogen production, chemical feedstock-based hydrogen production, and water electrolysis-based hydrogen production [30]. Among them, hydrogen produced through water electrolysis has the highest purity, such as alkaline water electrolysis (ALK), anion exchange membrane (AEM), proton exchange membrane (PEM), solid oxide electrolysis cell (SOEC) [31–34]. Mohe-bali et al. [35] conducted a comparative analysis of solid oxide electrolysis cell, polymer electrolyte membrane electrolysis cell, and alkaline electrolysis cell integrated in the same system to seek the optimal performance under different conditions, using exergy and economic analysis. Results showed that SOEC had the highest exergy efficiency and hydrogen production rate, while the cost is not the highest among the three. Kim et al. [36] conducted a techno-economic analysis of solid oxide electrolysis cell using a bottom-up model (BF model). The study highlights the sustainable strategy of SOEC that can expand the utilization of  $H_2$  in blast furnace. Therefore, SOEC is chosen as the device to implement hydrogen energy storage in the proposed hybrid system.

Based on the aforementioned considerations, numerous scholars have conducted individual research on SOFC-GT, SOEC, and CAES technologies, attempting to integrate them with other energy devices to address existing challenges and achieve higher efficiencies, the integration and coupling of multiple energy systems for supply have become a prominent trend in the future energy industry [37,38]. In this paper, the characteristics of hydrogen energy storage and its flexible

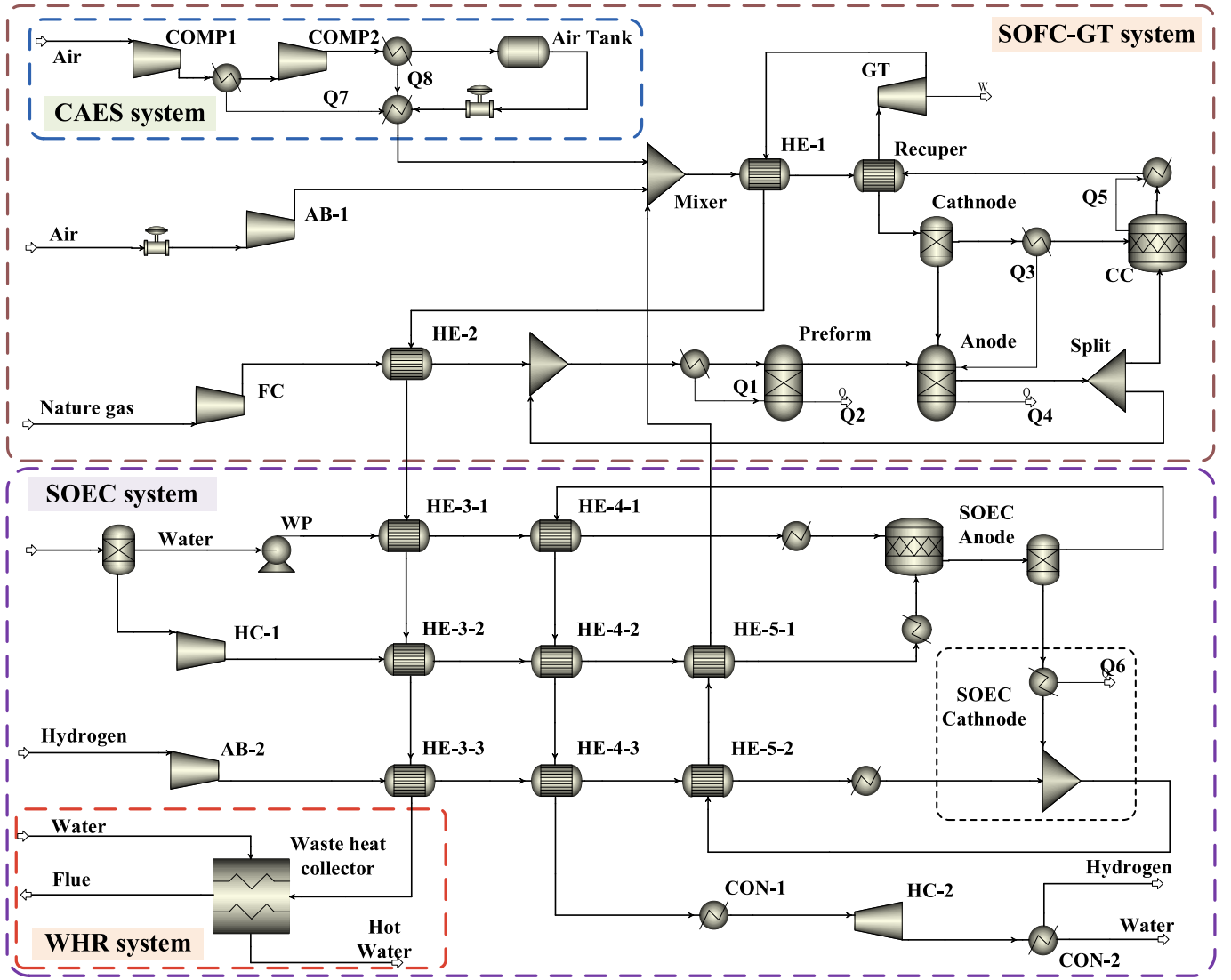


Fig. 2. Simulation model for the proposed hybrid system based on Aspen Plus.

conversion relationship with electricity are utilized, along with the similarities between compressed air energy storage and gas turbine units in terms of structure and working principles, to improve the optimization of power grid peak regulation. The integration of these three elements is based on the consideration of power production and consumption matching, breaking away from the traditional approach of separate supply-side energy provision and storage. The aim is to enhance power plant efficiency while achieving deep and flexible peak regulation. Moreover, the proposed hybrid power system ensures carbon-free emissions throughout the energy storage and release processes. The main advantages of the proposed concept are as follows:

- (1) By means of thermoelectric integration, the SOEC makes use of the electricity and heat created as a result of the SOFC functioning in order to balance out the discrepancy in energy production and consumption. In this context, SOFC serves as the primary power generation device, while the high-temperature exhaust gases are utilized by GT to harness the residual available energy. After the exhaust gases are released to atmospheric pressure, they are further utilized for auxiliary feed heating. This integrated approach facilitates cascaded energy utilization, and enhances the overall efficiency of the system while minimizing exergy losses.

- (2) The integration of compressed air energy storage and electrolytic hydrogen storage forms a dual energy storage structure, which effectively avoids the need to rely on the start-stop or operation deviation of conventional power plants to achieve deep peak regulation. This not only reduces environmental pressure by ensuring zero pollutant emissions during the process but also enhances the system's flexibility in peak regulation through SOEC. Additionally, the introduction of hydrogen production by SOEC fulfills the demand for hydrogen supply, promoting the development of the hydrogen industry and creating greater economic benefits.

The hybrid power system is evaluated in terms of thermodynamic energy, exergy, and economy, hoping that the proposed hybrid power system could provide a valuable reference for the efficiency improvement of power stations, the optimization of power grid peak regulation, and the promotion of hydrogen industry, and exert its application value.

## 2. System description

To enhance the production efficiency of gas power plants, optimize the flexibility of peak regulation, and promote the hydrogen industry, this paper proposes a novel hybrid power system design, as illustrated in

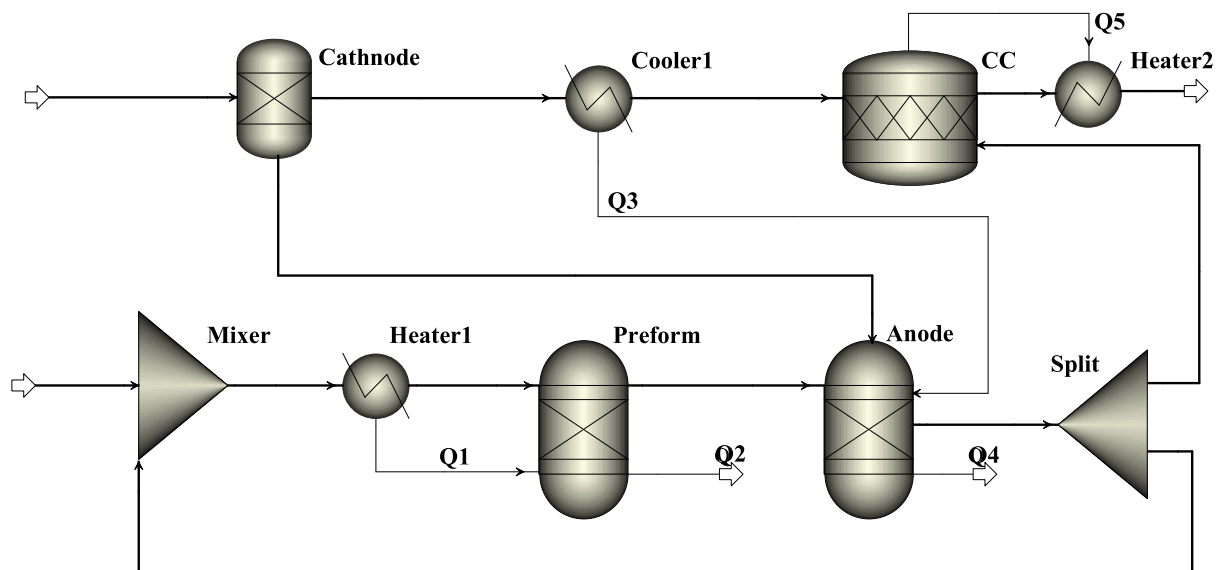


**Fig. 3.** Diagram of the SOFC simulation model based on Aspen Plus.

**Fig. 1:** the integration of conceptual compressed air and electrolytic hydrogen storage with SOFC-GT hybrid power system. This proposed scheme is built upon conventional gas power plants, incorporating SOFC system, SOEC system, and AA-CAES system. The aim is to achieve higher energy efficiency and cost-effectiveness while reducing greenhouse gas emissions.

The system utilizes conventional natural gas as the fuel, which is separately compressed with fresh air using compressors. The compressed gases then undergo sufficient heat exchange with the high-temperature flue gas at the gas turbine outlet. The fuel undergoes a reforming reaction in the SOFC to generate hydrogen and carbon monoxide. Subsequently, the chemical energy is directly converted into electrical energy through electrochemical reactions within the fuel cell [39]. An anode recirculation loop is implemented, directing partially unreacted gases back to the anode inlet. The remaining gases, along with the cathode outlet gas, are combined and directed into the combustion chamber, generating high-temperature flue gas that drives the gas turbine to produce power. The flue gas, still at a relatively high temperature and slightly above atmospheric pressure, is utilized for the first preheating of the inlet streams of both the SOFC-GT and SOEC subsystems. The three inlet streams of the SOEC subsystem undergo second and third preheating, then enter the electrolysis cell, where they undergo electrolysis to produce hydrogen and oxygen. The high-temperature, oxygen-rich air from the anode outlet is mixed with high-pressure air before entering the air preheater of the SOFC-GT system. The mixture (hydrogen and steam) from the cathode outlet completes the preheating task and is then pressurized and cooled through compressors and condensers. The cooled hydrogen is directed into the hydrogen storage tank, while the cooling water is recirculated to the water storage tank for reuse. During this process, the produced hydrogen can be sold as a commodity, generating economic benefits.

The compressed air subsystem employs an advanced adiabatic compressed air energy storage technology with thermal storage using heat transfer oil. It cools the high-pressure air between stages and after compression, storing the heat in high-performance thermal storage materials. This technology efficiently utilizes and stores energy during periods of low grid load, thereby enhancing energy utilization efficiency. During periods of low grid load, the CAES enters the energy storage phase, with the two-stage compressor operating to compress and store a certain amount of air in the air storage tank. When the grid demand peaks, the system enters the energy release phase. The pressure valve at the outlet of the air storage tank controls the release pressure,

and the pressurized air undergoes heat exchange with heat transfer oil to reach the same temperature as the high-pressure air at the outlet of the air compressor of the SOFC. This pressurized air then substitutes the original air inlet stream of the fuel cell, achieving peak shaving of the grid load. After calculating the grid load demand, a predetermined amount of hydrogen is introduced into the SOFC to increase the proportion of hydrogen in the fuel gas, thereby enhancing the power generation capacity of the system and achieving flexible peak regulation. During periods of basic grid load, only the fuel cell-gas turbine power system and the high-temperature water electrolysis system are in operation, while the compressed air energy storage system remains inactive.

### 3. Methodology

### 3.1. System simulation

Utilizing the Aspen Plus software's inherent operation unit module, rigorous thermodynamic property database, design specification setting, and calculator functionalities, the model building and process simulation of the proposed scheme in this paper are achieved [40]. The simulation model of the integrated system is presented in Fig. 2, where the SOFC-GT hybrid power system and the CAES system are simulated using the Peng-Robinson state equation, while the SOEC system process simulation adopts the Redlich-Kwong state equation of the electrolyte NRTL model [41].

### 3.1.1. Solid oxide fuel cell

The proposed scheme's main power output device is the SOFC-GT hybrid power subsystem. SOFC exhibits the potential for high electrical efficiency, as it directly converts the chemical energy of fuel into electricity or heat through electrochemical reactions. The waste heat from the SOFC at high temperatures can drive the gas turbine to generate power, forming a hybrid power generation system that improves the overall efficiency of gas-fired power plants [42]. As the Aspen Plus software does not have a model that can directly simulate the SOFC, a complete SOFC stack model is constructed with the help of an embedded Fortran program using an existing cell module [40]. The accuracy of the model is validated by comparing it with reference cases. The simulation process of SOFC is shown in Fig. 3.

Upon entering the fuel cell stack, the fresh fuel undergoes steam reforming (Eq. (1)) and water gas shift (Eq. (2)) reactions in the internal reforming module. Due to the endothermic nature of the reforming



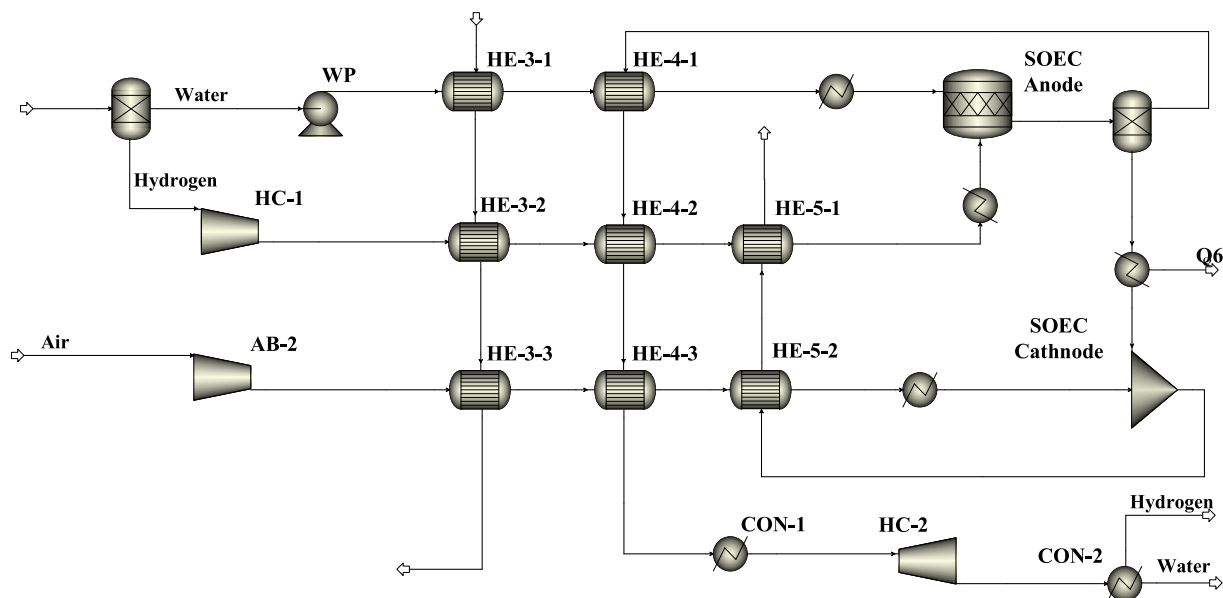
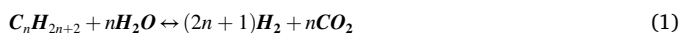


**Fig. 4.** Diagram of the SOEC simulation model based on Aspen plus.

reaction, significant temperature gradients are generated, necessitating the design of a pre-reformer. The 'PREFORM' module is employed to model this process. To ensure that the reforming process remains adiabatic, the heat absorbed by the reaction in the pre-reforming process is removed by the heat flow Q1, which is led from 'COOLER1' to the 'REFORMER'. To simulate the appropriate operating temperature for the reformer, the Design-spec function sets the heat load Q2 equal to zero [43,44].



The ‘Rgibbs’ reactor balance, the ‘Sep’ separator module, and the ‘Heater’ heat exchanger module are employed to simulate the anode and cathode reactions within the SOFC. The air flow entering the cathode module is separated according to the required oxygen demand ( $n_{O_2, required}$ ) of the fuel entering the anode module Eq. (4), and the process of oxygen ions migrating from the cathode to the anode is also designed and implemented in accordance with the Design-spec function.



$$n_{O_2,required} = 0.5 \times U_f \times (n_{H_2} + n_{CO} + 4 \times n_{CH_4} + 7 \times n_{C_3H_6} + 10 \times n_{C_3H_8} + 13 \times n_{C_4H_{10}}) \quad (4)$$

where  $n_{H_2}$ ,  $n_{CO}$ ,  $n_{CH_4}$ ,  $n_{C_2H_6}$ ,  $n_{C_3H_8}$ , and  $n_{C_4H_{10}}$ , represent the molar flow rate of the corresponding components in the fresh fuel stream of the SOFC, mol/s.

The calculation of the current ( $I$ , A) and current density ( $i_c$ , mA/cm<sup>2</sup>) generated by electrochemical reactions is given by Eq. (5) and Eq. (6) [40]:

$$I = 2 \times U_f \times F \times (n_{H_2} + n_{CO} + 4 \times n_{CH_4} + 7 \times n_{C_2H_6} + 10 \times n_{C_3H_8} + 13 \times n_{C_4H_{10}}) \quad (5)$$

$$i_c = \frac{n_{H_2} \times Ne \times F}{N \times A} \quad (6)$$

where  $U_f$  is the fuel utilization factor, which is set to 85% in this study [45].  $F$  is the Faraday constant, which is 96,485C/mol.  $N_e$  denotes the

number of electrons transferred in the reaction.  $N$  represents the number of individual cells, while  $A$  signifies the active area of an individual cell measured in square centimeters ( $\text{cm}^2$ ).

Calculation of cell voltage is a crucial aspect of SOFC modeling, in addition to current density. Eq. (7) expresses the difference between the actual operating voltage,  $V_{SOFC}$ , and the reference operating voltage,  $V_{ref}$ . The reference voltage is determined by the current density and is defined under reference conditions in the fuel cell manual, as shown in Eq. (8) [45].

$$V_{SOFC} = V_{ref} + \Delta V_n + \Delta V_T + \Delta V_{anode} + \Delta V_{cathode} \quad (7)$$

$$V_{ref} = 0.72988 + 2.00014 \times 10^{-4} \times i_c - 9.668 \times 10^{-7} \times i_c^2 + 2.626 \times 10^{-10} \times i_c^3 \quad (8)$$

The prediction of cell performance is achieved by implementing semi-empirical Eq. 9–12 using the Fortran program embedded in Aspen Plus [45,46].

(1) The operating pressure

$$\Delta V_p = 76 \times \log\left(\frac{P_{SOFC}}{P_{ref}}\right) \quad (9)$$

where  $P_{SOFC}$  represents the actual operating pressure (in bar) of the fuel cell, while  $P_{ref}$  is the reference operating pressure, which is set at 1 bar.

(2) The operating temperature

$$\Delta V_T = 0.008 \times (T_{SOFC} - T_{ref}) \times i_c \quad (10)$$

where  $T_{SOFC}$  is the operating temperature ( $^{\circ}\text{C}$ ) of the fuel cell, and  $T_{ref}$  is the reference operating temperature with a value of  $1000^{\circ}\text{C}$ .

(3) The partial pressure of hydrogen and steam

$$\Delta V_{anode} = 172 \times \log \left[ \frac{P_{H_2}}{P_{H_2O}} / \left( \frac{P_{H_2}}{P_{H_2O}} \right)_{ref} \right] \quad (11)$$

where  $P_{H_2}$  and  $P_{H_2O}$  represent the ratio of actual operating pressure of hydrogen and water vapor in the system.  $(P_{H_2}/P_{H_2O})_{ref}$  is the ratio of partial pressures of hydrogen and water vapor under reference condi-

**Table 1**

Model validation based on the 120 kW SOFC-GT hybrid system in Ref. [40,46].

Item	Ref. [40]	Ref. [46]	Simulation
Voltage (V)	0.70	0.69	0.69
Current density (mA/cm <sup>2</sup> )	178.00	179.08	179.08
Air utilization factor (%)	19.00	18.22	18.20
Outlet temperature of Pre-reformer (°C)	536.0	538.4	536.5
Anode outlet gas components (weight %)			
N <sub>2</sub>	5.10	5.14	5.14
H <sub>2</sub> O	50.90	50.87	50.87
CO <sub>2</sub>	24.90	24.96	24.96
H <sub>2</sub>	11.60	11.64	11.64
CO	7.40	7.40	7.39
Exhaust gas components (weight %)			
N <sub>2</sub>	77.30	77.36	77.37
O <sub>2</sub>	15.90	16.08	16.11
H <sub>2</sub> O	4.50	4.32	4.30
CO <sub>2</sub>	2.30	2.24	2.22
Exhaust gas temperature (°C)	834	–	831
Net generating capacity (kW)	119.30		119.23
AC efficiency in its entirety (%)	52.01		51.98

tions, where  $(P_{H_2}/P_{H_2O})_{ref}$  is equal to 0.15.

(4) The average partial pressure of oxygen in the cathode

$$\Delta V_{cathode} = 92 \times \log \left( \frac{P_{O_2}}{P_{O_2,ref}} \right) \quad (12)$$

where  $P_{O_2}$  represents the actual average oxygen partial pressure at the cathode during fuel cell operation, while  $P_{O_2,ref}$  represents the average oxygen partial pressure at the cathode under reference conditions,  $P_{O_2,ref}$  is 0.164.

The AC net power output of a fuel cell ( $W_{SOFC}$ , W) is the product of the cell voltage ( $V_{SOFC}$ , V) and current ( $I$ , A):

$$W_{SOFC} = V_{SOFC} \times I \times \eta_{DC-AC} \quad (13)$$

where  $\eta_{DC-AC}$  represents the direct current/alternating current conversion efficiency of the fuel cell power output. In this paper, a value of 0.92 is used based on the reference cited.

Therefore, the efficiency of the SOFC,  $\eta_{SOFC}$ , can be expressed as Eq. (14):

$$\eta_{SOFC} = \frac{W_{SOFC}}{m_{freshfuel} \times LHV_{fuel}} \quad (14)$$

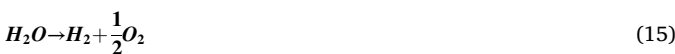
where  $m_{freshfuel}$  is the mass flow rate of the fuel, kg/s.  $LHV_{fuel}$  is the lower heating value of the fuel, kJ/kg.

The heat provided to the air stream by electrochemistry is calculated by the design specifications and transferred from 'Heater 1' to the 'anode' through the heat flow 'Q3', ensuring that the outlet temperatures of the anode and cathode are equal in the SOFC process. The chemical energy of the syngas is directly converted into electrical energy output by the fuel cell stack, while the remaining portion is converted into thermal energy to supply the endothermic reforming reaction or maintain the high-temperature conditions of the SOEC.

### 3.1.2. Solid oxide electrolysis cell

The SOEC displays a great capability in transforming electrical energy into chemical energy. Fig. 4 presents the simulation of the high-temperature solid oxide electrolysis model, with the primary electrochemical reactions being illustrated [47]:

Total reaction:



Negative electrode (positive electrode):



Positive electrode (hydrogen electrode):



where  $e^-$  represents the number of electrons transferred per mole of water electrolyzed into oxygen and hydrogen.

Therefore, the equation for calculating the current of the SOEC is as follows [48]:

$$I_{SOEC} = 2 \times n_{H_2O,react} \times F \times U_f \quad (18)$$

The hydrogen production through water electrolysis is an endothermic reaction, which requires a total energy input from both electrical energy ( $Q_{el}$ ) and thermal energy ( $Q_{th}$ ). The minimum electrical energy required for the reaction is equivalent to the change in the reaction's Gibbs free energy ( $\Delta G$ ). Under standard conditions (25 °C, 101.325 kPa), the reversible electromotive force of solid oxide electrolysis cell is related to  $\Delta G$ , as shown in Eq. (19). With the increase of operating temperature from ambient temperature to 800 °C,  $\Delta G^0$  decreases from 1.23 eV to 0.96 eV. As the operating temperature increases,  $\Delta G$  decreases, and high-quality electrical energy required for the process can be substituted by relatively low-quality thermal energy [48]. Compared with low-temperature electrolysis technology, high-temperature electrolysis technology requires less high-quality electrical energy.

$$\Delta G^0 = nFV_0 \quad (19)$$

In non-standard conditions, the possible electromotive force of the process for electrolyzing water to produce hydrogen can be obtained from the Nernst equation [10,49]:

$$V_{Nernst} = \frac{\Delta G}{2F} = \frac{\Delta G^0}{2F} + \left( \frac{RgT_{SOEC}}{2F} \right) \ln \left( \frac{P_{H_2}^{OUT} P_{O_2}^{OUT}}{P_{H_2O}^{OUT}} \right) + \eta_{ohm} + \eta_{act} + \eta_{conc} \quad (20)$$

where  $P_{H_2}$ ,  $P_{O_2}$  and  $P_{H_2O}$  are respectively the partial pressures of  $H_2$ ,  $O_2$  and  $H_2O$  during the operation of the electrolytic cell. Due to the electrolytic process, both cell and electrode have certain consumption,  $\eta_{ohm}$  indicating the loss caused by ion and electron conduction,  $\eta_{act}$  is the activation loss and the loss caused by reaction kinetics,  $\eta_{conc}$  is the concentration loss, indicating the loss caused by mass transmission.

Typically, to simplify the calculation of cell voltage, the ASR is used as an approximate value of the overpotential under cell current. The cell voltage calculation formula is rewritten as follows [48]:

$$V_{cell} = V_0 + (i_c \times ASR) \quad (21)$$

where  $i_c$  is the current density, mA/cm<sup>2</sup>. ASR mainly depends on the test material, manufacturing method and battery stack. In this paper, the value is 0.41 according to the reference case [48].

The formula for calculating the power required for electrolysis reaction is:

$$W_{SOEC} = V_{cell} \times I_{SOEC} \quad (22)$$

The expression for hydrogen production efficiency in SOEC can be described as follows:

$$\eta = \frac{\Delta H_{H_2}}{Q_{el} + Q_{th}} \quad (23)$$

where  $\Delta H_{H_2}$  is the high heat value of the prepared hydrogen, 285.8 kJ/mol [50].  $Q_{el}$  is equal to the sum of the power consumption of all pumps and compressors in the system and the electrical power required to electrolyze water.  $Q_{th}$  represents the sum of the heat energy supplied to SOEC [51].

### 3.1.3. Model validation

Table 1 presents a comparison of the data obtained from the 120 kW SOFC model simulated using Aspen Plus in this study and the design data

**Table 2**  
Basic parameter settings for SOEC model verification [48,52].

Item	Simulation
Cell temperature (°C)	848
Cell pressure (kPa)	100
H <sub>2</sub> O feed (g/h)	26.60
Absolute feed humidity, AH (%)	75
ASR (Ω·cm <sup>2</sup> )	0.41
steam conversion factor, SC (%)	85

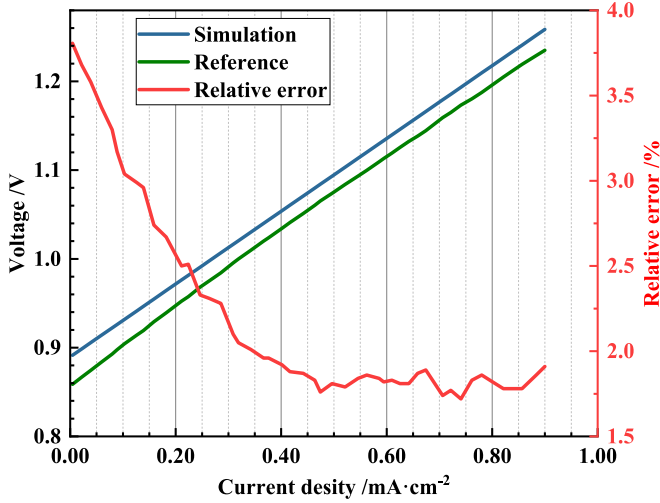


Fig. 5. Comparison of simulation results and experimental data.

from the reference literature [40,46]. The simulated values show good agreement with the design values in crucial parameters such as voltage, current density, power output, SOFC system efficiency, and gas composition ratios. It confirms the validity and reliability of the SOFC model built in this study.

Table 2 and Fig. 5 present a comparison between the simulation data obtained from the SOEC model constructed in this study using Aspen Plus and the experimental data reported in the literature. Under the same conditions of temperature, pressure, and inflow of imported supplies, the voltage-current density relationship curve is obtained through simulation, and the simulation results showed that the voltage-current density relationship curves plotted using the simulation and experimental values remained parallel when the current density is less than 1 mA/cm<sup>2</sup> [48]. Hence, in order to guarantee the dependability of the model data and achieve consistency between simulation and experimental values, a correction factor denoted as  $\alpha$  (0.98) is incorporated.

### 3.2. Model assumption

To determine the performance of the proposed hybrid power system and evaluate the advantages of the assessment scheme, thermodynamic energy and exergy analyses, as well as economic analyses, need to be conducted. To facilitate comparative research, the following basic assumptions are made regarding the simulation operating conditions in this study:

- It is assumed that the analyzed process is in thermodynamic equilibrium and a steady state.
- The environmental temperature is assumed to be 25 °C, and the atmospheric pressure is 101.325 kPa.
- The volume fraction of air composition is assumed to be 79% nitrogen and 21% oxygen.
- Assuming complete chemical reactions and neglecting adverse effects and electrode reactions.

- The effects of the surrounding environment are not considered, and losses of heat and mass, as well as changes in kinetic and potential energy, are ignored.

### 3.3. Energetic evaluation

Section 3.1 introduces the calculation methods of hydrogen production efficiency and the electrochemical efficiency of SOFC and SOEC host models, respectively. In this section, a comprehensive description of the various energy evaluation methods of the hybrid power system will be presented. In the proposed system presented in this paper, AA-CAES serves as an energy storage and peak regulation system. The compressor's air inlet flow rate is set to be consistent with the demand for fresh air intake from the fuel cell during the base compliance period. The system is charged during low power demand periods in the power grid. High-pressure air is released during high power demand periods, replacing the primary energy-consuming process of air compression in the SOFC-GT power system and achieving peak regulation [19]. Therefore, unless otherwise specified, the power or efficiency calculations below refer to those during the base compliance period.

For ease of expression and calculation, the sum of power consumed by the compressor, pump, and electrolytic cell in the system is denoted as  $W_{cons}$ , as shown in Eq. (24):

$$W_{cons} = W_{comp,SOFC} + W_{comp,SOEC} + W_{SOEC} + W_{CAES} \quad (24)$$

The present study proposes a novel hybrid power system, for which the net electrical power output and net efficiency are evaluated through the following equations:

$$W_{net} = W_{SOFC} + W_{GT} - W_{cons} \quad (25)$$

$$\eta_{net} = \frac{W_{net}}{\sum m_{fresh,in} \times LHV_{fresh,in}} \quad (26)$$

In addition to the electric power output, the hybrid system takes into account the energy contained in the high-purity hydrogen produced by the SOEC subsystem in the calculation of the total net power produced by the hybrid system:

$$W_{tot} = \Delta H_{H_2} + W_{net} \quad (27)$$

Thus, the overall energy efficiency of the proposed hybrid power system is:

$$\eta_{tot} = \frac{W_{tot}}{\sum m_{fresh,in} \times LHV_{fresh,in}} \quad (28)$$

### 3.4. Exergy evaluation

Exergy is a thermodynamic concept used to evaluate the efficiency of energy conversion processes. In terms of a specific state, it indicates the maximum theoretical work attainable by a system when it reaches equilibrium with a reference environment. Exergy analysis can be applied to various systems and aims to optimize energy use and reduce waste. By identifying the sources of exergy destruction or loss in a system, opportunities for improving efficiency and reducing energy consumption can be identified.

Based on this concept, an exergy analysis is performed on the new hybrid power generation system proposed in this study. Without considering the impacts of kinetic and potential energy, the effective energy of each material flow is composed of two parts: physical exergy ( $EX_{ms}^{ph}$ ) and chemical exergy ( $EX_{ms}^{ch}$ ) [53].

$$EX_{ms} = EX_{ms}^{ph} + EX_{ms}^{ch} \quad (29)$$

The chemical exergy of the incoming materials is calculated based on the elemental analysis, while the physical exergy is obtained by directly reading the physical properties of each flow stream from the Aspen Plus results. The effective energy calculation formula for the imported fuel,



**Table 3**  
Properties of the fuel for SOFC [45].

Item		Value
Composition (mole fraction, %)	N <sub>2</sub>	0.143
	CO	0.009
	CH <sub>4</sub>	0.813
	C <sub>2</sub> H <sub>6</sub>	0.029
	C <sub>3</sub> H <sub>8</sub>	0.004
	C <sub>4</sub> H <sub>10</sub>	0.002
Low heating value (MJ/kg)		38.450

**Table 4**  
Fundamental operating conditions and key parameter values employed in the hybrid system [45,48,56,57].

Item		Unit	Value
SOFC	Pressure of the reformer	bar	3.14
	Pressure of the SOFC in operation	bar	3.04
	Temperature at which SOFC functions	°C	910.00
	Utilization of fuel in SOFC	–	0.80
	Ratio of S/C	–	2.50
	Current density	mA/cm <sup>2</sup>	177.31
	Efficiency of DC/AC	%	92.00
	Active surface area of the SOFC	m <sup>2</sup>	96,100
	Anode recycling rate	%	61.15
	Thermal losses	%	2.00
GT	Pressure after expansion	bar	1.02
	Isentropic efficiency	%	85.00
	Mechanical efficiency	%	98.00
SOEC	Pressure of the SOEC in operation	bar	1.19
	Temperature of the SOEC in operation	°C	848.00
	Fuel utilization of SOEC	–	0.85
	Active area of cells stack	m <sup>2</sup>	200
	ASR	–	0.41
CAES	Current density	mA/cm <sup>2</sup>	609.46
	Inter-grade cooling temperature	°C	50.00
	Air storage temperature	°C	50.00
	First stage compression ratio	–	3.20
	Pressure of CAES vessel	bar	5.00
	Charging time	h	8.00
	Discharging time	h	8.00

**Table 5**  
Energy performance of the SOFC-GT subsystem.

Item		Unit	Value	Ref. [45]
Rate of fuel supply		kg/s	6.06	6.06
Rate of fuel supply air		kg/s	143.39	107.46
Current density		mA/cm <sup>2</sup>	177.31	177.31
Operating voltage		V	0.76	0.64
Net electricity generation of SOFC		MW	145.43	141.96
SOFC efficiency		%	57.42	55.29
Net output power of GT		MW	52.67	50.03
Consumption of auxiliary apparatus	Compressor (Air)	MW	21.94	–
	Compressor (Fuel)	MW	1.37	–
	Sum	MW	23.31	21.44
Total electric power generated		MW	198.09	191.99
Net electricity generation output		MW	174.79	170.55
Total SOFC-GT efficiency		%	75.01	73.19

due to its complex natural gas composition, is expressed as follows [54]:

$$EX_{gas} = m_{gas} \times LHV_{gas} \times (1.0064 + 0.1519 \times \frac{H}{C} + 0.0616 \times \frac{O}{C} + 0.0429 \times \frac{N}{C}) \quad (30)$$

**Table 6**  
Energy performance of the SOEC and CAES subsystem.

Item		Unit	Value
Amount of H <sub>2</sub> O supplied		kg/s	1.34
Amount of H <sub>2</sub> supplied		kg/s	0.05
Amount of air supplied		kg/s	0.80
Consumption power	Electricity for SOEC	MW	13.89
	Heat input	MW	15.70
Consumption of auxiliary apparatus	Air blower	MW	0.21
	Water pump	MW	0.001
	Compressor (H <sub>2</sub> to 5 bar)	MW	0.22
	Sum	MW	0.43
Rate of hydrogen production		kg/s	0.19
High heating value (H <sub>2</sub> )		kJ/mol	285.80
Energy of produced hydrogen		MW	25.33
Hydrogen production efficiency		%	85.23
AA-CAES			
Air feed rate		kg/s	143.39
Power consumption of compressor-1		MW	20.12
Power consumption of compressor-2		MW	7.49
Round-trip efficiency		%	79.46

where  $H$ ,  $C$ ,  $O$  and  $N$  are the amount of each corresponding component of the fuel.

The available energy ( $EX_{gas}$ , MW) of biogas with various gas compositions can be calculated as follows [55]:

$$EX_{gas} = m_{gas} \times \sum [n_i \times (ex_{i,ph} + ex_{i,ch} + RT_0 \times \ln n_i \sum n_i)] \quad (31)$$

where  $m_{gas}$  is the mass flow of gas material, kg/s.  $n_i$  is the molar yield of gas component  $i$ , kmol/kg.  $ex_{i,ph}$  and  $ex_{i,ch}$  are the physical and chemical exergy of gas component  $i$ , kJ/kmol, respectively.  $R$ , the universal gas constant, is 8.314 kJ/kmol·K.  $T_0$  is the ambient temperature.

The effective energy balance of components or systems in steady-state processes in the proposed hybrid power system can be described as follows [46]:

$$\sum EX_{in} + \sum W_{in} + \sum Q_{in} = \sum EX_{out} + \sum W_{out} + \sum Q_{out} + \sum EX_{des} \quad (32)$$

where  $\sum EX_{in}$  and  $\sum EX_{out}$  are total input and total output, and the unit is MW.  $\sum W_{in}$  and  $\sum W_{out}$  are total work input and total work output, MW.  $\sum Q_{in}$  and  $\sum Q_{out}$  are total heat input and total heat output, MW.  $\sum EX_{des}$  is the total effective energy loss, MW.

### 3.5. Economic evaluation criteria

Economic analysis is a crucial process for evaluating the economic feasibility of a power plant project. It requires consideration and analysis of multiple factors to determine the economic feasibility and return on investment of the project. Based on the thermodynamic analysis results, the economic evaluation of the new design is conducted by means of manual calculations, utilizing the dynamic payback period (DPP, years) and net present value (NPV, k\$) as indicators to evaluate the economic performance of the new design. DPP is negatively correlated with the project's profitability, meaning that the shorter the DPP, the higher the profitability of the project. NPV is commonly used in the financial field to calculate the net present value of cash flows throughout the project's life cycle, which is obtained by subtracting the present value of cash outflows from the present value of cash inflows. This indicator considers the time value and risk of cash flows, and it can help evaluate the investment value and feasibility of the project. The calculation formula is as follows [46]:

$$\sum_{y=1}^{DPP} \frac{C_{in} - C_{out}}{(1 + i_{dis})^y} = 0 \quad (33)$$

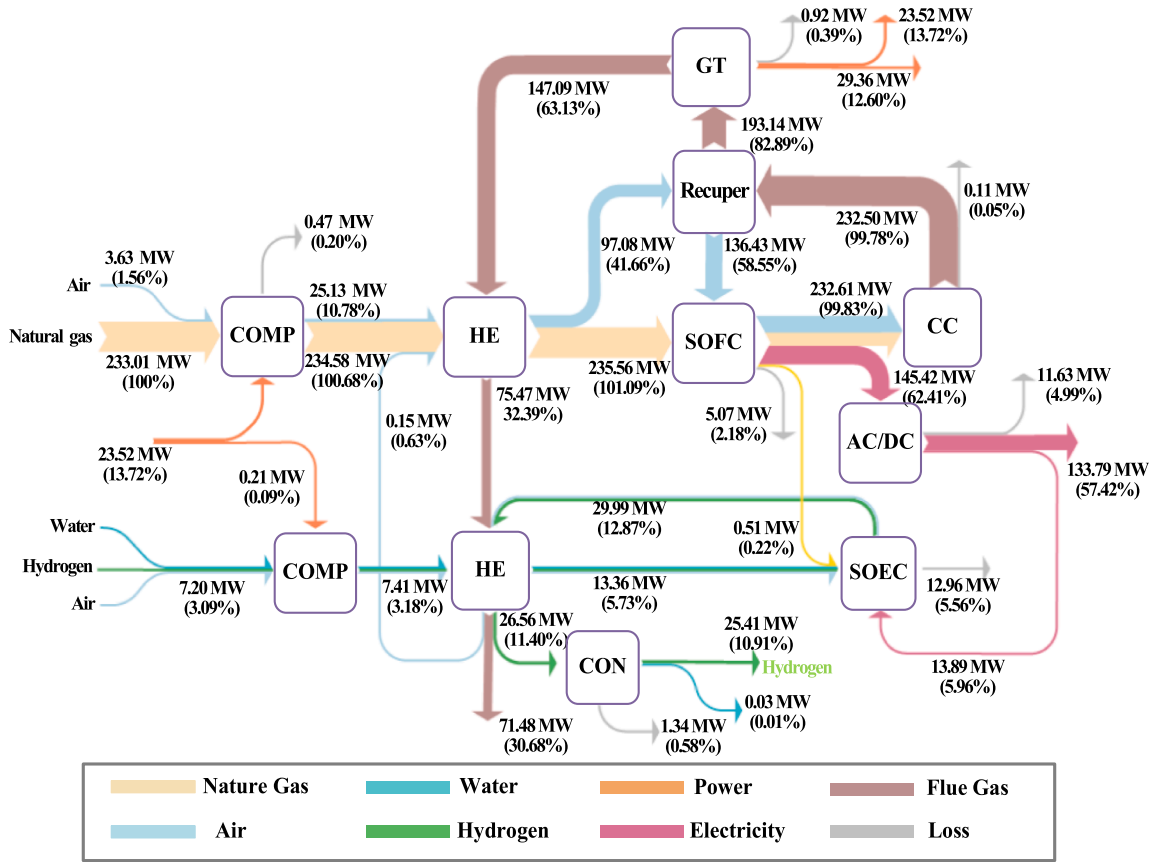


Fig. 6. Energy flow diagram of the proposed hybrid system in the basic time.

where  $y$  denotes the specific year within the project's duration. The variables  $C_{in}$  and  $C_{out}$  indicate the cash inflow and outflow in the corresponding year, respectively, and are measured in k\$. The parameter  $i_{dis}$  represents the discount rate, which is used to evaluate the present value of future cash flows [46].

$$NPV = \sum_{y=1}^k \frac{(C_{in} - C_{out})}{(1 + i_{dis})^y} \quad (34)$$

where  $k$  is the plant lifetime, year.

## 4. Results and discussion

### 4.1. Parameters of proposed system

The proposed hybrid power system in the present study employs natural gas as the primary feedstock. The gas composition and LHV of the feedstock before entering the SOFC are demonstrated in Table 3.

The new hybrid power system proposed in this paper employs natural gas as the primary fuel source. Table 4 presents the basic operational parameters of the system. The fuel and air at ambient pressure are first compressed by the FC and AB to 3 bar, respectively, to meet the operating pressure requirements of the SOFC. After preheating, the fuel enters the SOFC at a temperature of approximately 200 °C and reaches around 580 °C after reforming inside the fuel cell, while the air enters the fuel cell at a temperature of 865 °C. The SOFC directly converts a portion of the chemical energy of the fuel into electrical energy, while the remaining energy is converted into heat, which is used to absorb the endothermic reforming reactions and to preheat the inlet fuel. The temperature difference between the inlet fuel and air is compensated by the electrochemical reaction, with a heat flow ( $Q_5$ ) from the 'Heater 1' block to the 'Anode' block. The heat flow ( $Q_5$ ) is calculated using a

design specification calculator, which ensures a constant temperature of 910 °C at the cathode and anode outlets. When the input materials are maintained under certain conditions, the voltage of the fuel cell stack stabilizes at 0.76 V, and the current density is 177.31 mA/cm<sup>2</sup>. There exist some unreacted gases at the anode outlet, so a portion of the synthetic gas is extracted and fed back to the anode to increase efficiency and the temperature of the fresh inlet materials, while the remaining gases containing combustibles are sent to the combustion chamber for combustion. The heat released during this process is used for GT power generation. Assuming a fuel utilization rate of 80% for the fuel cell, an isentropic expansion efficiency of 85% for the GT, and the mechanical efficiency of the GT and the GE are assumed to be 98% and 99%, respectively.

The feedstock for the SOEC subsystem is compressed and pressurized by compressors and water pumps to the operating pressure of 1.19 bar. The feedstock inlet temperature is 15 °C, except for air, which enters at ambient temperature. The feedstock is then heated to 650 °C through heat exchange with multiple high-temperature streams. The required energy for the electrolysis reaction is supplied by the SOFC. The SOEC and SOFC share a thermal chamber, and the heat loss from the SOFC subsystem heats the electrolysis inlet material from 650 °C to the operating temperature of the SOEC (848 °C) [56]. While maintaining the inlet conditions for the SOEC feedstock, the current density stabilizes at 609.46 mA/cm<sup>2</sup>, and the corrected voltage is 1.12 V.

To ensure that the air stream 68 released during the energy release stage of the CAES system has the same thermodynamic properties as stream 13, a storage pressure of 5 bar and a storage temperature of 50 °C is set. Moreover, it is assumed that the charging and discharging time are both 8 h per day.

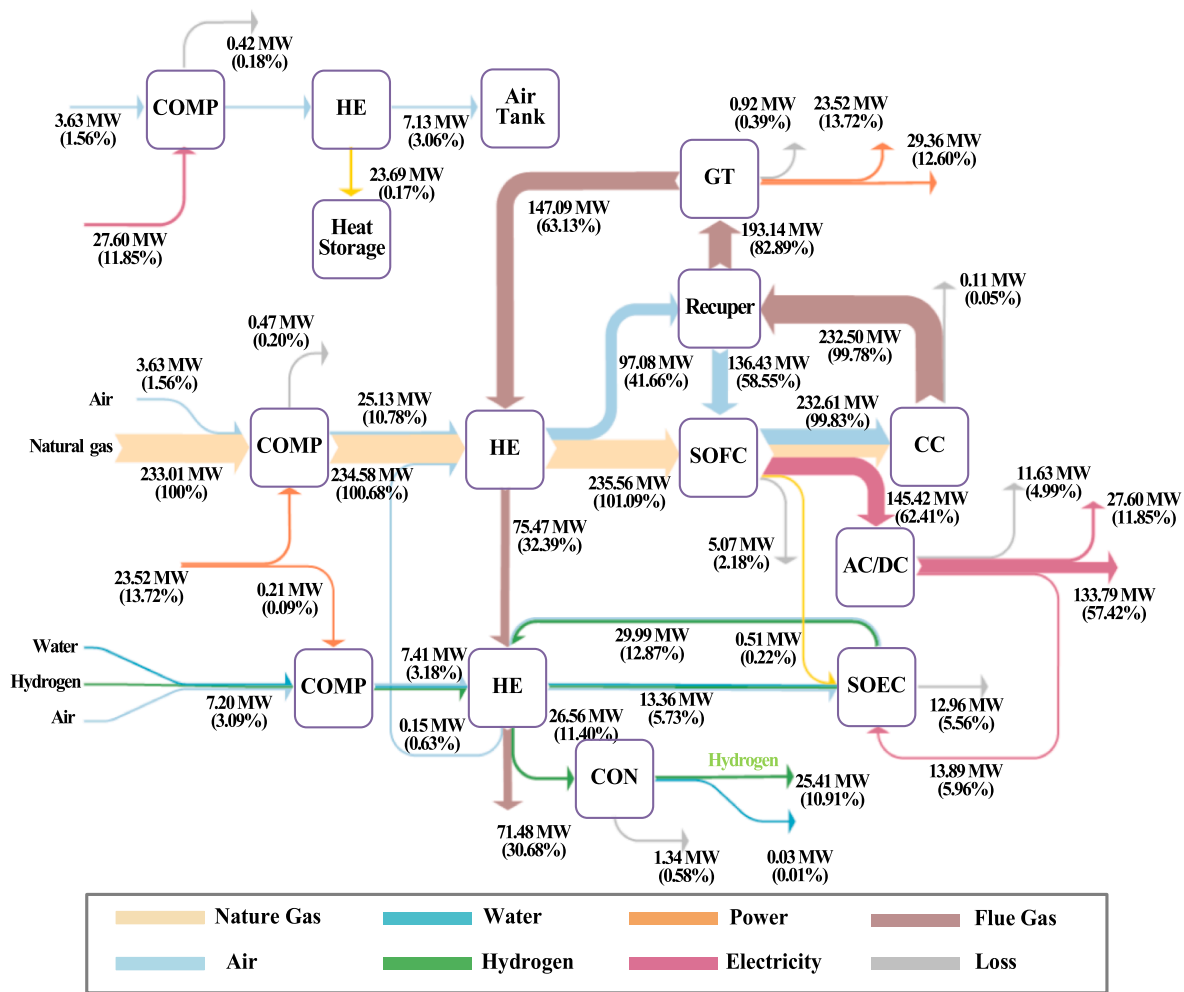


Fig. 7. Energy flow diagram of the proposed hybrid system in the charging time.

#### 4.2. Energy analysis

Energy analysis is a methodology used to investigate the energy conversion process and the work done by the system with different forms of energy. By analyzing the energy variation and the environmental energy changes can provide insights into the energy changes of the system. The thermodynamic and economic analysis of the system allows to obtain the energy performance of the integrated system simulated by the system model, as shown in Table 5-6.

Table 5 presents a comparison of the performance data between the proposed hybrid power system and the case unit for the SOFC-GT while ensuring the same current density of the SOFC. By maintaining the fuel supply rate of the hybrid system (natural gas, 6.06 kg/s) and changing the fresh air flow rate to 143.39 kg/s, although the compressor power consumption increased by 1.87 MW, the power generation of the SOFC increased by 3.47 MW and the power output of the GT increased by 2.64 MW. As a result, the overall energy output efficiency of the SOFC-GT section increased by 1.82% compared to the case unit. On the basis of this, the air flow rate of the compressed air system is set to be consistent with the SOFC, and the water flow rate of the SOEC system is 1.34 kg/s, while the flow rates of hydrogen and air are 0.05 kg/s and 0.80 kg/s, respectively. The total power generated by the hybrid power system is 188.46 MW, of which 133.79 MW is generated by the SOFC, and the GT generates the remaining 52.67 MW. Moreover, the power consumption of all auxiliary equipment of the hybrid system is borne by the power generation from the GT section, which is 23.31 MW. The heat and electricity required by the electrolytic cell of the SOEC are provided by

the SOFC, which is in the same shared heat box as the SOEC. At rated conditions, 13.89 MW of electric power generated by the SOFC subsystem is utilized for water electrolysis, and 15.70 MW of thermal energy is delivered to the electrolysis tank of the SOEC. Table 6 shows the energy analysis results of the SOEC and CAES. Additionally, the overall hydrogen production rate of the hybrid system is 0.19 kg/s, and the hydrogen production efficiency of the hybrid power system reaches 85.23%, which is within the efficiency range required by the SOEC.

In order to rigorously scrutinize the energy allotment of the entire system, E Sankey produced Figs. 6-8, which describes the energy of each flow in detail. Taking the input energy of 233.01 MW of the mixed system fuel as the reference value (100%), the fresh fuel and air undergo compression, heat exchange, and other processes, which generate 145.43 MW of direct current electricity by SOFC, and are converted to 133.79 MW of alternating current electricity. The SOFC incurs an energy loss of 7.94 MW. The high-temperature flue gas (187.02 MW) generated by the combustion of waste fuel gas in the combustion chamber drives the GT to produce additional power (52.67 MW), of which 23.31 MW is supplied to the plant's compressors, and the remaining 29.36 MW represents the net electrical power generated by the GT. The high-temperature flue gas at the outlet of the GT still contains a significant amount of energy (147.09 MW), which is utilized for heating the fresh fuel in the hybrid power system. Due to the need for SOEC, the electricity generated by SOFC is converted to AC power, of which 13.89 MW is used for electrolysis. Moreover, since SOFC and SOEC share a thermal box, 15.82 MW of heat is directly supplied to the electrolytic cell of SOEC. The energy contained in the hydrogen gas generated by the

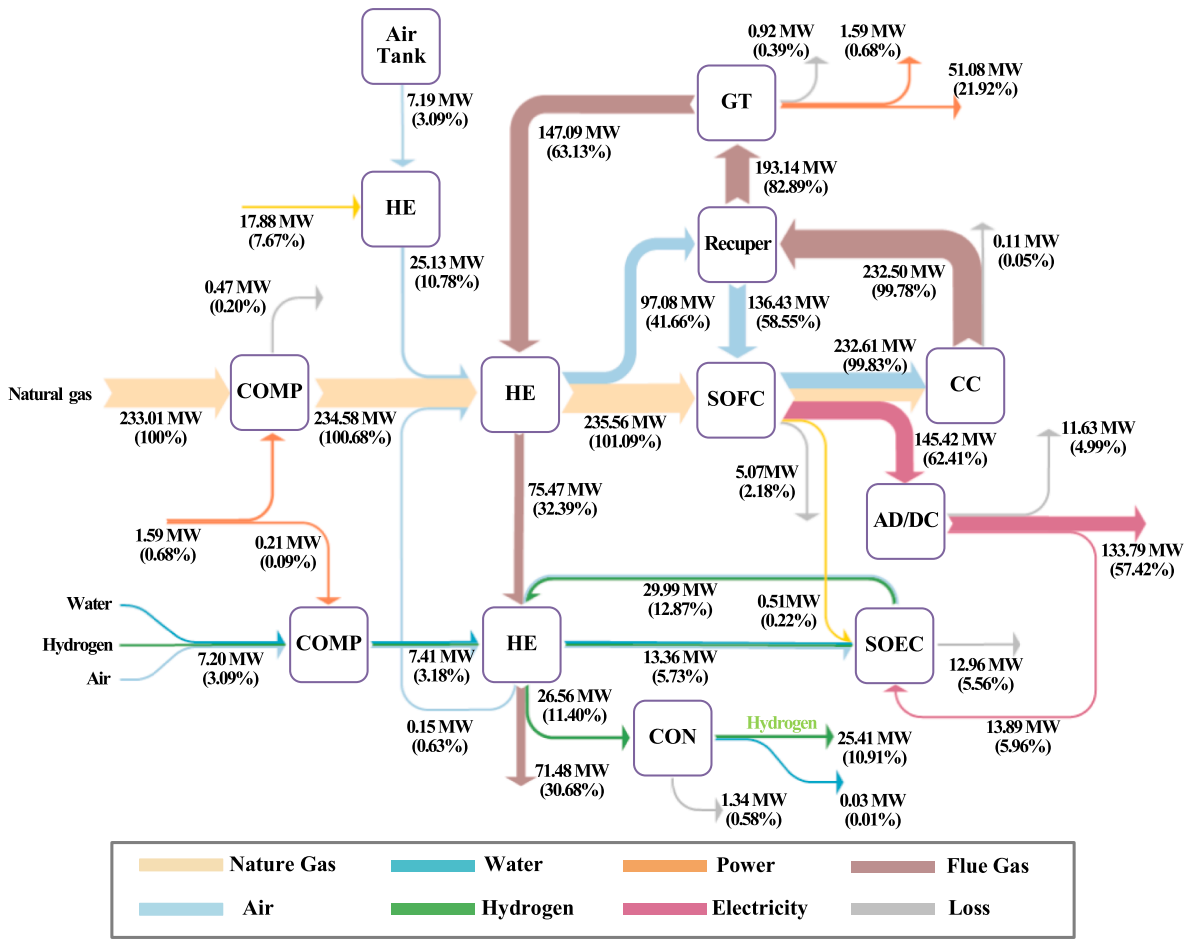


Fig. 8. Energy flow diagram of the proposed hybrid system in the discharging time.

Table 7

Energy comparison at different time periods.

Item	Value (MW)		
	Basic time (100% Design condition)	Charging time (80% Design condition)	Discharging time (115% Design condition)
SOFC	+133.79	+133.79	+133.79
GT	+52.67	+52.67	+52.67
Comp of SOFC	-23.31	-23.31	-1.37
SOEC	-14.32	-14.32	-14.32
AA-CAES	-	-27.61	-
Energy of the produced hydrogen	+25.33	+25.33	+25.33
Net electric power production of the proposed hybrid system	148.83	121.22	170.76
Net electric efficiency	63.87%	52.02%	73.29%
Total power production of the proposed hybrid system	174.15	146.55	196.09
Total energy efficiency	74.74%	62.89%	84.16%

electrolytic reaction is 25.33 MW. To further optimize the waste heat recovery in the system, a novel scheme is proposed to recover waste heat from the flue gas (71.48 MW) and utilize it for domestic hot water generation, with cold water serving as the cooling source. The net electricity efficiency of the new hybrid power system reaches over 60%, with net power output generated by GE (29.07 MW) and SOFC (119.47

MW).

Assuming that the peak and off-peak periods of the power grid load demand are each 8 h per day, this study compares the CAES system's energy production and electricity consumption during the charging and discharging periods with the basic load period, as shown in Table 7. During the period when the CAES is not operating, the net electricity generation of the hybrid power system is 148.83 MW, with a net electrical efficiency of 63.87%, which increases to an overall energy efficiency of 74.74% when the energy produced by the hydrogen is taken into account. During the power grid load demand off-peak period, the CAES system enters the charging state, consuming an additional power of 27.61 MW. The hybrid power system operates at 80% load, with a net power output of 121.22 MW. The CAES system enters the discharging state during the peak load demand periods. The hybrid power system operates at 115% load, with a net electricity generation of 170.76 MW. The energy storage cycle efficiency of the conceptual advanced adiabatic CAES system is 79.46%. The SOEC system operates unchanged, and there is almost no change in the energy flow during the basic load period, which can be ignored [58]. As shown in Figs. 6-8, a comparison analysis of the energy flow of the power plant during different load regulation periods only requires additional energy analysis of the CAES subsystem, while the energy flow of other subsystems remains unchanged.

When the depth of load following in the CAES system is insufficient, the SOEC can assist load following by controlling its current density by adjusting the feed rate. When the electricity demand of the grid is too high for the CAES system to supply enough energy, the target output power of the SOFC can be set according to Fig. 9. The additional hydrogen produced by the SOEC can be fed into the SOFC via a formula

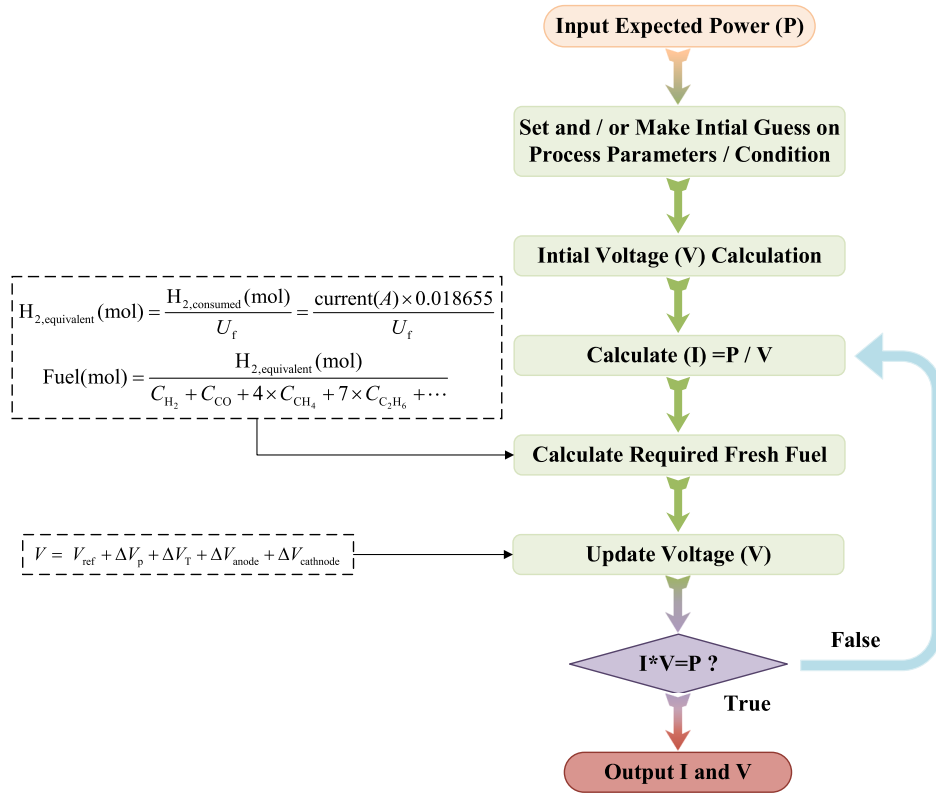


Fig. 9. SOFC computational flowchart.

Table 8

Exergy analysis of the proposed hybrid power system under basic load conditions.

Item		Basic time	
		MW	Ratio
Exergy input (Natural gas)		240.78	97.34%
Exergy input (H <sub>2</sub> )		5.83	2.35%
Exergy input (H <sub>2</sub> O)		0.64	0.26%
Exergy input (Air)		0.12	0.05%
Total exergy input (Fuel)		247.37	100%
Gross exergy output (Electricity) of SOFC-GT		178.92	72.33%
Gross exergy output (Heat) of the produced H <sub>2</sub>		21.03	8.50%
Gross total exergy output		199.95	80.83%
Net total exergy output		162.32	65.62%
Exergy losses			
SOFC-GT	Compressor	3.66	1.48%
	Heat exchanger	8.52	3.44%
	Solid oxide electrolysis cell	37.26	15.06%
	Combustion chamber	15.54	6.28%
	Gas turbine	2.51	1.01%
Sum		67.48	27.28%
SOEC	Heat exchanger	2.10	0.85%
	Compressor & Pump	0.02	0.01%
	Solid oxide electrolysis cell	15.04	6.08%
	Condenser	0.37	0.15%
	Compressor (H <sub>2</sub> )	0.02	0.01%
Sum		17.56	7.10%
Total exergy loss		85.04	34.38%
Exergy efficiency of SOFC-to-electricity		74.31%	
Exergy efficiency of SOEC		58.12%	
Total exergy efficiency (%)		65.62%	

calculation to satisfy the fuel demand and achieve the target output power, thereby achieving grid flexibility in load following.

#### 4.3. Exergy analysis

The present study conducted a comprehensive thermodynamic analysis of the hybrid power system. The results of the thermodynamic analysis are summarized in Table 8. The reasons and locations for the degradation of energy quality within the system are analyzed in detail by analyzing the thermodynamic performance. Based on the analysis results, the difficulties are resolved, thereby achieving the goal of improving the overall system efficiency. In this hybrid power system, the supply rate of the raw materials remains constant. Thus, the exergy input of the system from the imported raw materials remains unchanged. The exergy of all the imported streams in the system (247.37 MW) is set as the reference value of 100%. The fraction of thermodynamic losses attributed to the SOFC is the largest, with a value of 37.26 MW, representing 15.06 % of the total exergy. This is because the chemical exergy of the anode side flow has a significant impact on the irreversibility of the cell stack. The irreversibility of the SOFC has the highest contribution to the thermodynamic losses in the hybrid power system, followed by the SOEC (15.04 MW), which represents a relative exergy fraction of 6.08%. As shown in Fig. 10, the sum of the exergy losses in the SOFC and SOEC systems accounts for 63.34% of the total exergy losses in the hybrid power system.

In addition, the overall exergy output of the system is 162.31 MW, with a comprehensive exergy conversion efficiency of 65.62%. The exergy efficiency of the proposed hybrid power system in this study is superior to that of typical gas-fired power plants, owing to the higher quality of energy produced by the system and the efficient stepwise utilization of energy, which significantly enhances the exergy efficiency.



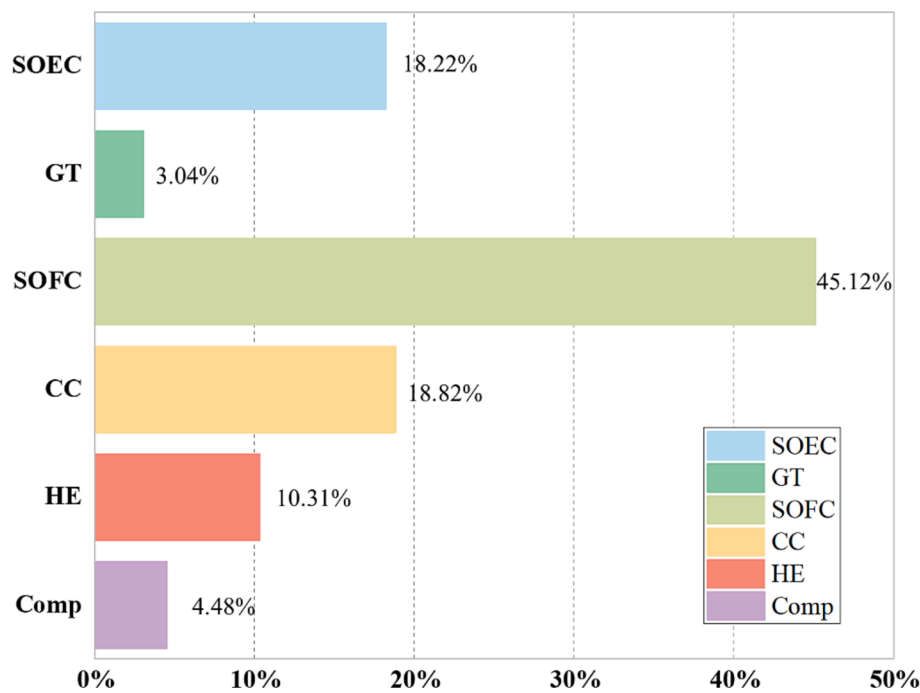


Fig. 10. Exergy destruction ratio of different sections in the proposed hybrid power system.

Table 9

Fundamental assumptions and data for the economic evaluation.

Item		Unit	Value
Total annual operational hours [59]		h	7200
Project duration	Building phase	year	2
[59]	Economic phase	year	23
Feed-in tariff [60]	Basic period	\$/MWh	95.9
	Peak period	\$/MWh	142.9
	valley period	\$/MWh	50.3
Price of fuel [61]		\$/t	27.33
Price of water [62]		\$/t	0.62
Hot water fees [62]		\$/t	3.08
Hydrogen price [63]		\$/t	3258.43
Fees for operation and management [59]		k\$	10% of total investment cost
Discount rate [59]		%	10

#### 4.4. Economic evaluation

As presented in Table 9, the basic parameters for economic evaluation are determined based on relevant references. It is assumed that the proposed hybrid power system will operate for 7200 h annually, with a lifespan of 25 years. The annual operating and maintenance cost is 10% of the investment cost. The on-grid electricity prices are 142.9, 95.9, and 50.3 \$/MWh for peak, base, and valley load periods, respectively. The hydrogen price is 3258.43 \$/t, the industrial water price is 0.62 \$/t, and the price of selling hot water is 3.08 \$/t. The discount rate, chosen as 10%, determines the present value of future cash flow in the discounted cash flow analysis [59].

The suggested hybrid power system's overall expense includes investment and maintenance operation costs. The project's profit mainly relies on electricity, hydrogen, and hot water sales. The equipment investment cost is estimated by the cost function approach or scale factor method in Table 10, and the estimated equipment investment cost is listed in Table 11. The total investment amount for the project is 282103.97 k\$, where SOFC-GT, SOEC, CAES, and WHR systems account for 86.35%, 11.85%, 1.62%, and 0.18%, respectively, as shown in Figs. 11 and 12.

Table 12 presents the economic benefits of the suggested hybrid

power system. During the commercial period, the operation and maintenance cost for the power plant is 28210.40 k\$ per year, with an annual electricity output of 105.79 GWh, an annual hydrogen production of 5978.79 t, and an annual supply of  $4.6 \times 10^6$  t of hot water. The total annual revenue from selling electricity, hydrogen, and hot water is 107452.53 k\$, 19481.47 k\$, and 7556.15 k\$, respectively. The net income per year is 102069.89 k\$. The primary investment for the project is 282103.97 k\$, and the construction period is two years. The capital can be recovered 3.81 years after the project is completed considering discounted cash flows. The net present value of the project, calculated for a 25-year project operation period, is 492275.82 k\$. The above data indicate that the proposed hybrid power system based on gas-fired power plants has great economic feasibility. The incorporation of the hydrogen production system not only aligns with the trend of carbon reduction (with low carbon emissions of 0.08 ~ 0.12 t/GJ) but also yields additional profits to the project.

#### 5. Parametric analysis

##### 5.1. Influence of SOFC operating temperature

The effect of changing the operating temperature of the SOFC from 800 °C to 1200 °C on the overall power generation and energy efficiency of both the SOFC subsystem and the hybrid power system, scaled down proportionally by a factor of ten, is presented in Fig. 13. As the temperature increases, the SOFC output power decreases from 13.42 MW to 12.92 MW, while the GT output power increases from 5.66 MW to 5.84 MW. The total energy output power of the hybrid power system shows a decreasing trend, but there is a maximum value in the increasing range between 900—1000 °C. Considering the material limitations of the SOFC operating temperature and minimizing the loss of the fuel cell stack, the operating temperature of the SOFC subsystem in this study is set at 910 °C to ensure stable operation.

##### 5.2. Influence of SOFC current density

The current density is a critical parameter during the operation of SOFC, as it has a significant impact on their performance and lifespan. In

**Table 10**  
Estimation methods for investment costs of proposed integrated system.

Component		Unit	Function	Source	
Cost function method					
SOFC-GT hybrid system	Cell stacks	\$	$A_{SOFC} \times N_{SOFC} \times (2.96 \times T_{SOFC} - 1907)$	[46]	
	Auxiliary	\$	$0.1 \times Z_{SOFC}$	[46]	
	Inventor	\$	$10^5 \times \left(\frac{W_{SOFC,DC}}{500}\right)^{0.7}$	[46]	
	Gas turbine	\$	$1318.5 \times W_{GT} - 98.328 \times \ln W_{GT}$	[64]	
	Combustion chamber	\$	$\frac{46.08 \times m_{oxidant}}{0.995 - \frac{P_{out}}{P_{in}}} \times e^{\frac{18}{1000}T_{out} - 26.4} + 1$	[65]	
Generator		\$	$60 \times (P_{nom})^{0.95}$	[46]	
SOEC	Water pump	\$	$3 \times \left[ 422 \times (W_{WP})^{0.71} \times 1.41 \times \left(1 + \frac{1 - 0.8}{1 - \eta_{WP}}\right) \right]$	[66]	
	Electrolytic cell	\$	$Z_{SOEC} = 2285 \times W_{SOEC}$	[10]	
CAES	Air tank	\$	$1.218 \times e^{[2.631 + 1.3673 \times (\ln V_{Airtank}) - 0.06309 \times (\ln V_{Airtank})^2]}$	[67]	
	Oil tank	\$	$5941.7 \times (A_{Oil\ tank})^{-0.389}$	[68]	
Heat exchanger		\$	$130 \times \left(\frac{A_{HE-x}}{0.093}\right)^{0.78}$	[46]	
Air preheater		\$	$12000 \times \left(\frac{A_{APH}}{100}\right)^{0.6}$	[57]	
Scaling up method					
Component	Basic cost (\$)	Basic scale	Scale parameter	Scaling factor	Source
Compressor	91,652	445	power output (kW)	0.67	[46]
Condenser	1400	20.83	Flow rate (t/h)	0.8	[69]

**Table 11**  
Component investment costs in the proposed integrated system.

Equipment	Cost (k\$)
SOFC-GT hybrid system	Fuel compressor
	Air blower
	SOFC
	SOFC auxiliary
	Gas turbine
	Combustion chamber
	Generator
	Heat exchanger-1
	Heat exchanger-2
	SOEC
SOEC	Water pump
	Air blower
	Hydrogen compressor-1
	Sum of Heat exchanger-3, 4, 5
	Condenser
WHR	Hydrogen compressor-2
	Hydrogen storage tank
	Water heat collector
	Compressor-1
	Compressor-2
CAES	HE-6
	HE-7
	HE-8
	Air tank
	Oil tank
Sum	282103.97

a similar manner, the effect of scaling down the size of the proposed hybrid power system by a factor of ten on the output power and efficiency of the SOFC is investigated. With the increase in current density, the net electrical efficiency of SOFC decreased by 1.09%. This is attributed to the elevation of temperature caused by high current density, which results in a lower conversion rate of fuel chemical energy into electrical energy, an increase in exothermic heat of electrochemical

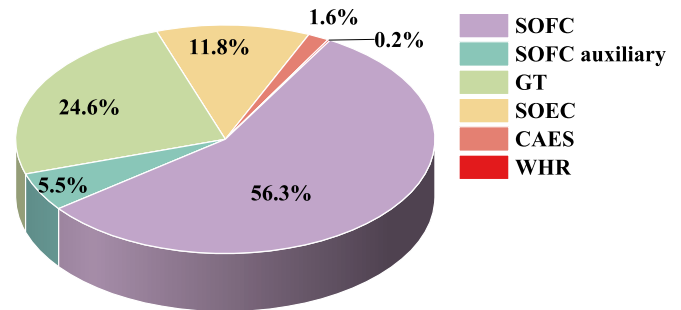


**Fig. 11.** Investment cost proportion of hybrid system.

reaction, and an increase in thermal stress and corrosion rate of the materials, thereby shortening the lifespan of SOFC. Furthermore, at high current density, the polarization resistance of SOFC also increases, which limits the further increase of current density. Since the power generation efficiency of SOFC is considerably higher than that of other common power cycles, the net electrical output efficiency of the hybrid power system is significantly affected by the current density. In Fig. 14, as the current density increases from 170 to 215 mA/cm<sup>2</sup>, the net electrical output efficiency of the hybrid power system declines from 62.89% to 61.80%. Therefore, by controlling the current density reasonably, the efficient operation and long-term stability of SOFC can be achieved.

### 5.3. Influence of SOEC operating temperature

Based on Fig. 15, it can be observed that the open circuit voltage of the electrolyzer is inversely correlated with temperature. The required electrolysis voltage at different current densities exhibits the same relationship, consistent with the predicted trend by the Nernst equation. The linear relationship between current density and voltage at low

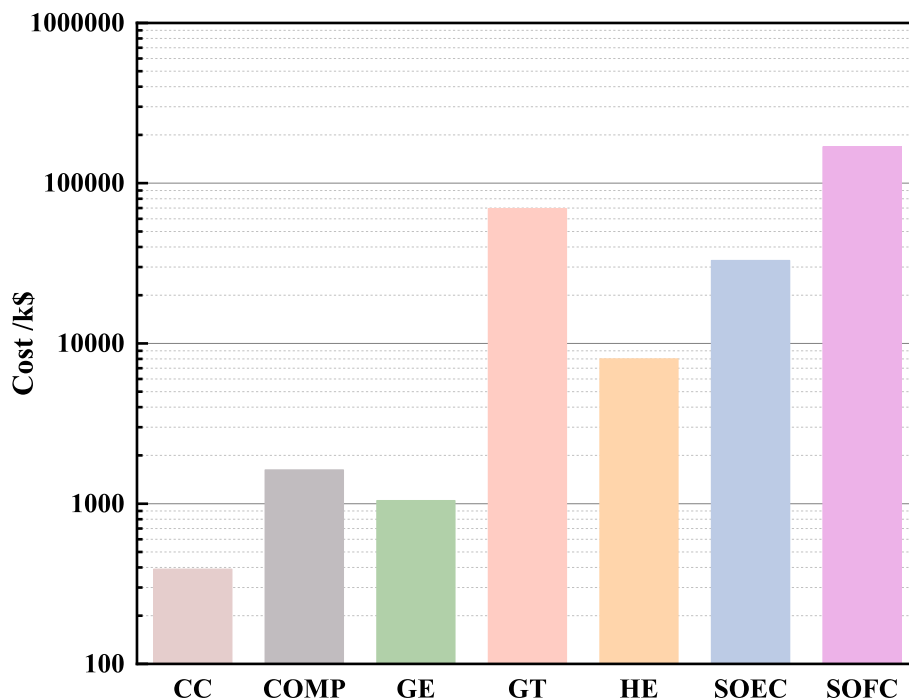


Fig. 12. Investment cost of different sections in the proposed hybrid power system.

Table 12

Economic evaluation outcomes of the suggested hybrid system.

Item	Unit	Value
Annual electricity production	GWh	105.79
Annual hydrogen production yield	t	5978.79
Annual supply of domestic hot water (DHW)	t	4607409.60
Annual electricity sales revenue	k\$	107452.53
Annual hydrogen sales revenue	k\$	19481.47
Annual DHW sales revenue	k\$	7556.15
Annual operating and maintenance cost	k\$	282103.97
Yearly transportation expenses	k\$	195.80
Dynamic payback period	year	5.81
Net present value	k\$	492275.82

current densities is mainly due to the focus of this study on system integration to enhance energy efficiency, the calculation of kinetic losses is simplified using the Area Specific Resistance (ASR) based on thermodynamic equilibrium. Additionally, as an oxygen-ion conductor, the electrolyte's conductivity decreases at high temperatures, further reducing Ohmic losses. Therefore, higher temperatures are commonly employed in practice to minimize activation overpotential and Ohmic overpotential, thereby reducing ASR, simulating lower voltage losses, and improving hydrogen production efficiency.

## 6. Conclusions

A hybrid power system based on integrated fuel cells, water electrolysis, and conceptual compressed air energy storage technology is designed for a gas turbine power plant, which achieves multi-generation of hydrogen, heat, and electricity. The performance of the proposed hybrid power system is evaluated by a comprehensive analysis of the thermodynamic energy, exergy, and economics, and the influence of essential parameters on the system performance is discussed. Based on the research results, the following conclusions are drawn:

- (1) Compared with the traditional high-temperature solid oxide fuel cell (SOFC) coupled with the gas turbine (GT) power plant case model, the SOFC-GT power system has a total energy output

power of 198.09 MW and a total energy efficiency of 75.01%. When the feed amount is constant, and the grid demand is at the basic load period, a net power output of 141.29 MW can be generated, with an efficiency of 60.64%. Taking into account the latent heat contained in the hydrogen produced, the efficiency can reach up to 71.51%.

- (2) Replacing the waste heat boiler of the reference unit with compressed air energy storage and electrolysis units results in a slight decrease in net electricity output power but avoids the need to change the unit's operating conditions to achieve peak shaving. The SOFC stack and the SOEC electrolysis cell share the heat source in a common thermal box, allowing the waste heat dissipated during SOFC operation to be recovered and improving the efficiency of the SOEC while generating additional hydrogen to increase the economic benefits of the power plant. Even during periods of low power demand, a net electricity efficiency of 48.79% can be achieved, far surpassing that of traditional gas-fired power plants. The exhaust gas is fed into the WHR system to heat domestic water, further improving the energy utilization efficiency and achieving cascading energy utilization.
- (3) It is found that the exergy efficiency is 65.62%, and the total exergy loss is 85.04 MW. Further analysis shows that the SOFC, combustion chamber, and SOEC have the most considerable exergy losses in the hybrid power system, accounting for 45.12%, 18.82%, and 18.22%, respectively. The reactions that occur in these components cause significant changes in the chemical exergy of the working fluids, resulting in enormous exergy destruction.
- (4) During periods of high grid load, the net electricity output power under full load conditions is 163.23 MW, with a net electricity efficiency of 70.05%. The total energy output reaches 188.55 MW, with a total energy efficiency of 80.92%. By analyzing the electricity prices at different times and considering the revenue from selling hydrogen and supplying hot water, the proposed system is estimated to have a net present value of 492275.82 k\$ over a 25-year project life, with a dynamic payback period of 5.81 years. Excluding the 2-year construction period, the system can be paid back in 3.81 years and has low carbon emissions of

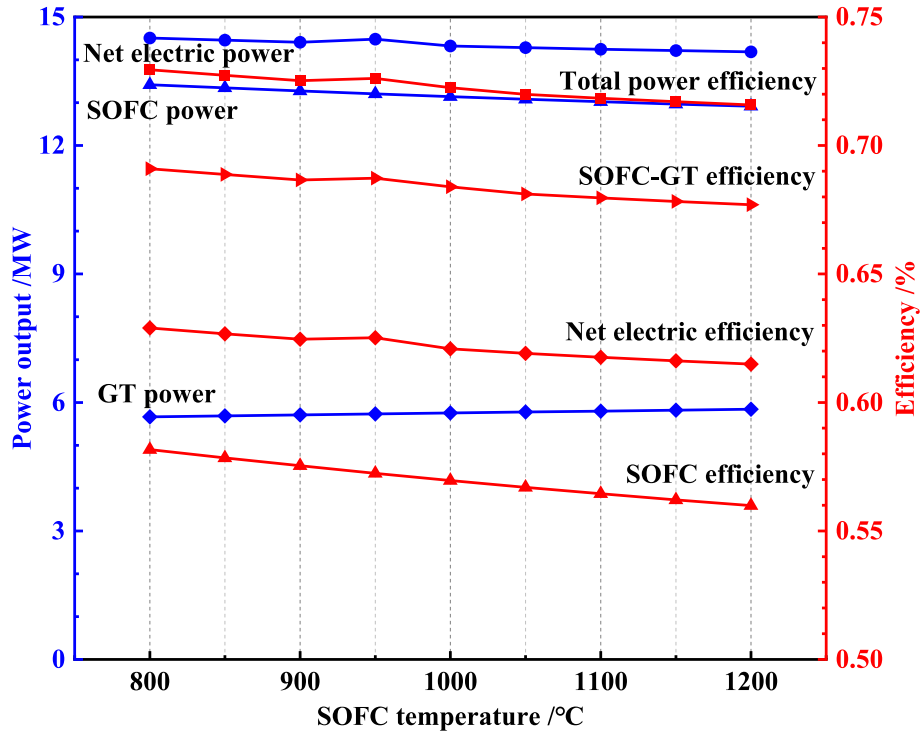


Fig. 13. Influence of the SOFC operating temperature on the performance of the proposed hybrid system.

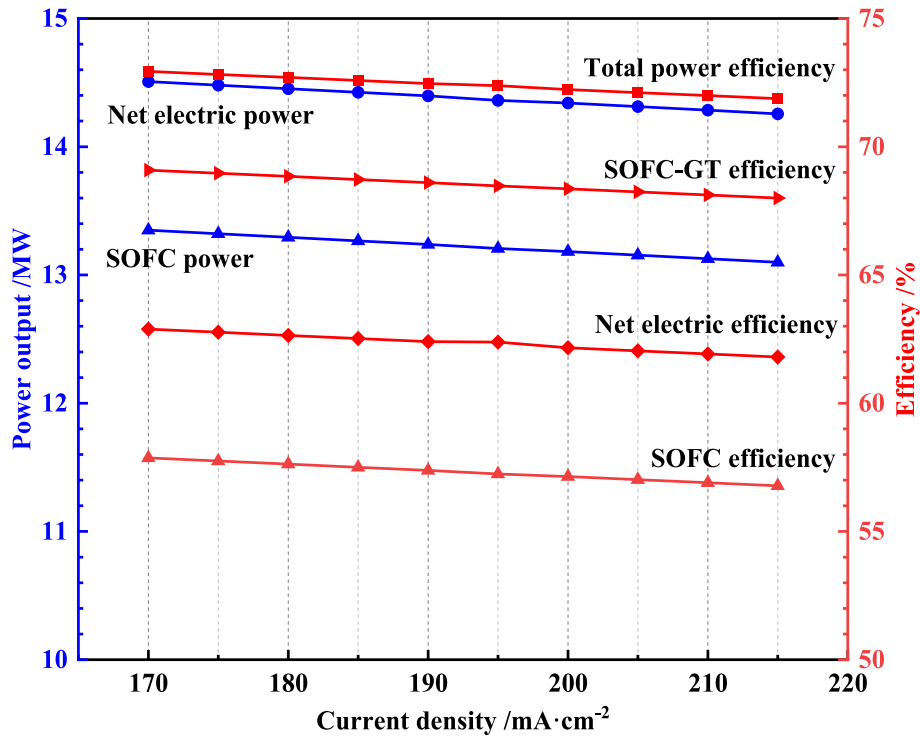


Fig. 14. Influence of the SOFC current density on the performance of the proposed hybrid system.

0.08 ~ 0.12 t/GJ. Therefore, the design of this hybrid power system is also very suitable in terms of economic and environmental sustainability.

Currently, renewable energy power generation alone cannot meet the world's energy demand. Therefore, there will be an increasing trend towards multi-system integration in the future. The proposed solution in

this paper fills the gap in the market for traditional fossil fuel power plants that require deviating from their operating design conditions to achieve peak shaving while also enabling hydrogen production. Future research will focus on achieving flexible operation, further optimizing efficiency, and providing feasible strategies.

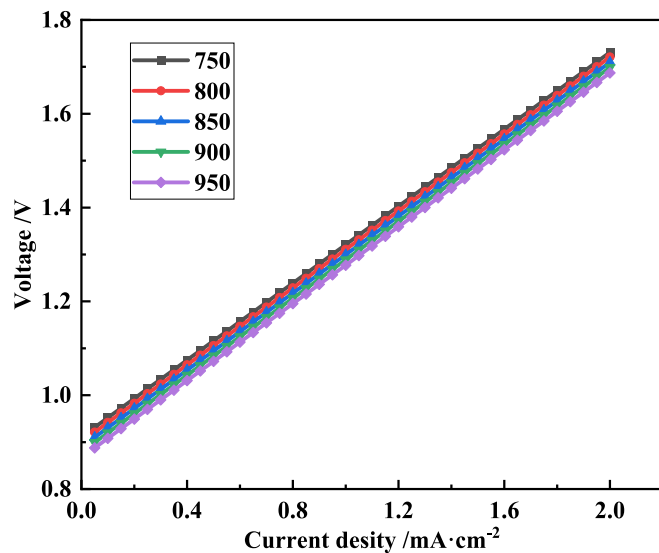


Fig. 15. Influence of the SOEC operating temperature on the performance.

### CRedit authorship contribution statement

**Bo Li:** Conceptualization, Methodology, Formal analysis, Writing – original draft. **Heng Chen:** Methodology, Software, Formal analysis, Writing – original draft. **Jinhang Li:** Software, Validation, Formal analysis. **Wenchao Li:** Conceptualization, Writing – review & editing, Supervision. **Peiyuan Pan:** Software, Validation, Formal analysis. **Lining Wu:** Writing – review & editing, Supervision. **Gang Xu:** Validation, Writing – review & editing.

### Declaration of Competing Interest

The authors declare that they have no known competing financial interests or personal relationships that could have appeared to influence the work reported in this paper.

### Data availability

No data was used for the research described in the article.

### Acknowledgements

This work was supported by the National Science Fund of China (No. 52276006 and No. 52106008).

### References

- Violetto G, Noro M, Colbertaldo P, et al. Enhancement of energy generation efficiency in industrial facilities by SOFC-SOEC systems with additional hydrogen production. *Int J Hydrogen Energy* 2019;44:9608–20.
- Feng Z, Niu W, Wang W, et al. A mixed integer linear programming model for unit commitment of thermal plants with peak shaving operation aspect in regional power grid lack of flexible hydropower energy. *Energy (Oxf)* 2019;175:618–29.
- Obara S. Economic performance of an SOFC combined system with green hydrogen methanation of stored CO<sub>2</sub>. *Energy (Oxf)* 2023;262:125403.
- Kim Y, Lee J, Cho H, et al. Novel cryogenic carbon dioxide capture and storage process using LNG cold energy in a natural gas combined cycle power plant. *Chem Eng J* 2023;456:140980.
- Weber A. Fuel flexibility of solid oxide fuel cells. *Fuel Cells (Weinh)* 2021.
- Wang X, Hou R. Comparison and analysis of heat exchange and off-gas recycle strategies in tri-reforming-SOFC system. *Int J Hydrogen Energy* 2023.
- Wang X, Lv X, Weng Y. Performance analysis of a biogas-fueled SOFC/GT hybrid system integrated with anode-combustor exhaust gas recirculation loops. *Energy (Oxf)* 2020;197:117213.
- Xia M, Yao S, Ying C. Analysis and multi-objective optimization of SOFC/GT/SCO<sub>2</sub> hybrid power system based on thermodynamics and economics. *Appl Therm Eng* 2023;232:121033.
- Huang Y, Turan A. Fuel sensitivity and parametric optimization of SOFC-GT hybrid system operational characteristics. *Therm Sci Eng Prog* 2019;14:100407.
- Chitgar N, Emadi MA. Development and exergoeconomic evaluation of a SOFC-GT driven multi-generation system to supply residential demands: Electricity, fresh water and hydrogen. *Int J Hydrogen Energy* 2021;46:17932–54.
- Pirkandi J, Penhani H, Maroufi A. Thermodynamic analysis of the performance of a hybrid system consisting of steam turbine, gas turbine and solid oxide fuel cell (SOFC-GT-ST). *Energy Convers Manag* 2020;213:112816.
- Liu Y, Han J, You H. Performance analysis of a CCHP system based on SOFC/GT/CO<sub>2</sub> cycle and ORC with LNG cold energy utilization. *Int J Hydrogen Energy* 2019;44:29700–10.
- Wang Z, Chen H, Xia R, et al. Energy, exergy and economy (3E) investigation of a SOFC-GT-ORC waste heat recovery system for green power ships. *Therm Sci Eng Prog* 2022;32:101342.
- Zhou X, Chen W, Zhang B. Proposed hybrid system with integrated SOFC, gas turbine, and compressor-assisted absorption refrigerator using [mmim]DMP/CH<sub>3</sub>OH as working fluid. *Energy (Oxf)* 2022;261:125301.
- Vojdani M, Fakhari I, Ahmadi P. A novel triple pressure HRSG integrated with MED/SOFC/GT for cogeneration of electricity and freshwater: Techno-economic-environmental assessment, and multi-objective optimization. *Energy Convers Manag* 2021;233:113876.
- Ouyang T, Zhao Z, Zhang M, et al. A micro off-grid power solution for solid oxide fuel cell waste heat reusing enabled peak load shifting by integrating compressed-air energy storage. *Appl Energy* 2022;323:119589.
- Koohi-Fayegh S, Rosen MA. A review of energy storage types, applications and recent developments. *J Energy Storage* 2020;27:101047.
- Yang S, Zhang Z, Ji Q, et al. Study on the water temperature distribution characteristics of a mixed pumped storage power station reservoir: A case study of Jinshuitan Reservoir. *Renew Energy* 2023;202:1012–20.
- Roushenas R, Razmi AR, Soltani M, et al. Thermo-environmental analysis of a novel cogeneration system based on solid oxide fuel cell (SOFC) and compressed air energy storage (CAES) coupled with turbocharger. *Appl Therm Eng* 2020;181:115978.
- Han Z, Ma F, Wu D, et al. Collaborative optimization method and operation performances for a novel integrated energy system containing adiabatic compressed air energy storage and organic Rankine cycle. *J Energy Storage* 2021;41:102942.
- Huang L, Guo H, Xu Y, et al. Influence of design point on off-design and cycling performance of compressed air energy storage systems-from key processes to the whole system. *J Energy Storage* 2023;57:106181.
- Wang Q, Duan L, Lu Z, et al. Thermodynamic performance comparison of SOFC-MGT-CCHP systems coupled with two different solar methane steam reforming processes. *Int J Hydrogen Energy* 2023.
- Neuwirth M, Fleiter T, Manz P, et al. The future potential hydrogen demand in energy-intensive industries - a site-specific approach applied to Germany. *Energy Convers Manag* 2022;252:115052.
- Zhang Q, Chen W, Ling W. Policy optimization of hydrogen energy industry considering government policy preference in China. *Sustain Prod Consum* 2022;33:890–902.
- Dumbrell NP, Wheeler SA, Zuo A, et al. Public willingness to make trade-offs in the development of a hydrogen industry in Australia. *Energy Policy* 2022;165:112987.
- Gao X, An R. Research on the coordinated development capacity of China's hydrogen energy industry chain. *J Clean Prod* 2022;377:134177.
- Genovese M, Schlüter A, Scionti E, et al. Power-to-hydrogen and hydrogen-to-X energy systems for the industry of the future in Europe. *Int J Hydrogen Energy* 2023.
- Beasy K, Lodewyckx S, Mattila P. Industry perceptions and community perspectives on advancing a hydrogen economy in Australia. *Int J Hydrogen Energy* 2023;48:8386–97.
- Amoco B. bp Energy edition Outlook. 2023. p.
- Shiva Kumar S, Lim H. An overview of water electrolysis technologies for green hydrogen production. *Energy Rep* 2022;8:13793–813.
- Patil V, Reshmi PV, Prajna S, et al. Degradation mechanisms in PEM fuel cells: A brief review. *Materials Today: Proceedings* 2023.
- Sebbahi S, Nabil N, Alaoui-Belghiti A, et al. Assessment of the three most developed water electrolysis technologies: Alkaline water electrolysis, proton exchange membrane and solid-oxide electrolysis. *Mater Today: Proc* 2022;66:140–5.
- Palmas S, Rodriguez J, Mais L, et al. Anion exchange membrane: A valuable perspective in emerging technologies of low temperature water electrolysis. *Curr Opin Electrochem* 2023;37:101178.
- Min G, Choi S, Hong J. A review of solid oxide steam-electrolysis cell systems: Thermodynamics and thermal integration. *Appl Energy* 2022;328:120145.
- Mohebbali Nejadian M, Ahmadi P, Houshfar E. Comparative optimization study of three novel integrated hydrogen production systems with SOEC, PEM, and alkaline electrolyzer. *Fuel (Lond)* 2023;336:126835.
- Kim J, Lee H, Lee B, et al. An integrative process of blast furnace and SOEC for hydrogen utilization: Techno-economic and environmental impact assessment. *Energy Convers Manag* 2021;250:114922.
- AlZahrani AA, Dincer I. Modeling and performance optimization of a solid oxide electrolysis system for hydrogen production. *Appl Energy* 2018;225:471–85.
- Hoettecke L, Thiem S, Schäfer J, et al. Resilience optimization of multi-modal energy supply systems: Case study in German metal industry. *Comput Chem Eng* 2022;162:107824.



- [39] Bao C, Wang Y, Feng D, et al. Macroscopic modeling of solid oxide fuel cell (SOFC) and model-based control of SOFC and gas turbine hybrid system. *Prog Energy Combust Sci* 2018;66:83–140.
- [40] Zhang W, Croiset E, Douglas PL, et al. Simulation of a tubular solid oxide fuel cell stack using AspenPlus<sup>TM</sup> unit operation models. *Energy Convers Manag* 2005;46:181–96.
- [41] Wang Y, Chen H, Qiao S, et al. A novel methanol-electricity cogeneration system based on the integration of water electrolysis and plasma waste gasification. *Energy (Oxf)* 2023;267:126490.
- [42] Zhang X, Li J, Li G, et al. Cycle analysis of an integrated solid oxide fuel cell and recuperative gas turbine with an air reheating system. *J Power Sources* 2007;164:752–60.
- [43] Habibollahzade A, Gholamian E, Houshfar E, et al. Multi-objective optimization of biomass-based solid oxide fuel cell integrated with Stirling engine and electrolyzer. *Energy Convers Manag* 2018;171:1116–33.
- [44] Songfeng T, Zhengkuan LI, Yaxuan L, et al. Thermal performance analysis of calcium cycle carbon capture process based on SOFC-GT-ST combined cycle power system. *Electric Power Science and Engineering* 2021;37:37–46.
- [45] Duan L, Huang K, Zhang X, et al. Comparison study on different SOFC hybrid systems with zero-CO<sub>2</sub> emission. *Energy (Oxf)* 2013;58:66–77.
- [46] Peng W, Chen H, Liu J, et al. Techno-economic assessment of a conceptual waste-to-energy CHP system combining plasma gasification, SOFC, gas turbine and supercritical CO<sub>2</sub> cycle. *Energy Convers Manag* 2021;245:114622.
- [47] An H, Liu Z, Mu S. Process analysis of a novel coal-to-methanol technology for gasification integrated solid oxide electrolysis cell (SOEC). *Int J Hydrogen Energy* 2023;48:9805–11.
- [48] Schefold J, Brisse A, Poepeke H. Long-term steam electrolysis with electrolyte-supported solid oxide cells. *Electrochim Acta* 2015;179:161–8.
- [49] Zhang Q, Chen H, Li B, et al. A novel system integrating water electrolysis and supercritical CO<sub>2</sub> cycle for biomass to methanol. *Appl Therm Eng* 2023;225:120234.
- [50] Bolt A, Dincer I, Agelin-Chaab M. Energy and exergy analyses of hydrogen production process with aluminum and water chemical reaction. *Energy (Oxf)* 2020;205:117978.
- [51] Chenjia Z, Jun C, Yukui Z, et al. Simulation of high temperature solid oxide water electrolysis for hydrogen production based on thermodynamic equilibrium. *Acta Energiae Solaris Sinica* 2021;42:210–7.
- [52] Chenjia Z. Analysis and simulation of hydrogen production from water electrolysis by high temperature solid oxides. North China Electric Power University; North China Electric Power University(Beijing); 2021.
- [53] Guo Y, Yu Z, Li G, et al. Performance assessment and optimization of an integrated solid oxide fuel cell-gas turbine cogeneration system. *Int J Hydrogen Energy* 2020;45:17702–16.
- [54] Chen H, Zhang M, Xue K, et al. An innovative waste-to-energy system integrated with a coal-fired power plant. *Energy (Oxf)* 2020;194:116893.
- [55] Yu D, Hu J, Wang W, et al. Comprehensive techno-economic investigation of biomass gasification and nanomaterial based SOFC/SOEC hydrogen production system. *Fuel (Lond)* 2023;333:126442.
- [56] Mehrpooya M, Bahnamiri FK, Moosavian SMA. Energy analysis and economic evaluation of a new developed integrated process configuration to produce power, hydrogen, and heat. *J Clean Prod* 2019;239:118042.
- [57] Xue X, Li J, Liu J, et al. Performance evaluation of a conceptual compressed air energy storage system coupled with a biomass integrated gasification combined cycle. *Energy (Oxf)* 2022;247:123442.
- [58] Razmi A, Soltani M, Aghanajafi C, et al. Thermodynamic and economic investigation of a novel integration of the absorption-recompression refrigeration system with compressed air energy storage (CAES). *Energy Convers Manag* 2019;187:262–73.
- [59] Khallaghi N, Jeswani H, Hanak DP, et al. Techno-economic-environmental assessment of biomass oxy-gasification staged oxy-combustion for negative emission combined heat and power. *Appl Therm Eng* 2021;196:117254.
- [60] Han Z, Sun Y, Li P. Thermo-economic analysis and optimization of a combined cooling, heating and power system based on advanced adiabatic compressed air energy storage. *Energy Convers Manag* 2020;212:112811.
- [61] Al-Khori K, Bicer Y, Boulfrad S, et al. Techno-economic and environmental assessment of integrating SOFC with a conventional steam and power system in a natural gas processing plant. *Int J Hydrogen Energy* 2019;44:29604–17.
- [62] An J, Yan D, Deng G, et al. Survey and performance analysis of centralized domestic hot water system in China. *Energy Buildings* 2016;133:321–34.
- [63] Zhang G, Wan X. A wind-hydrogen energy storage system model for massive wind energy curtailment. *Int J Hydrogen Energy* 2014;39:1243–52.
- [64] Kumar P, Singh O. Thermoeconomic analysis of SOFC-GT-VARS-ORC combined power and cooling system. *Int J Hydrogen Energy* 2019;44:27575–86.
- [65] Roy D, Samanta S, Ghosh S. Performance assessment of a biomass-fuelled distributed hybrid energy system integrating molten carbonate fuel cell, externally fired gas turbine and supercritical carbon dioxide cycle. *Energy Convers Manag* 2020;211:112740.
- [66] Morgan ER, Manwell JF, McGowan JG. Opportunities for economies of scale with alkaline electrolyzers. *Int J Hydrogen Energy* 2013;38:15903–9.
- [67] Jiang R, Yin H, Peng K, et al. Multi-objective optimization, design and performance analysis of an advanced trigenerative micro compressed air energy storage system. *Energy Convers Manag* 2019;186:323–33.
- [68] Peng L, Qingya H, Zhonghe H. Study on thermal economy of two AA-CAES+CSP systems. *Acta Energiae Solaris Sinica* 2022;43:424–32.
- [69] Li J, Wang H, Chen H, et al. Comparative thermodynamic and techno-economic analysis of various medical waste-to-hydrogen/methanol pathways based on plasma gasification. *Appl Therm Eng* 2023;221:119762.